Radar Observations of Tornado-Warned Convection Associated with Tropical Cyclones over Florida

STEVEN M. MARTINAITIS[a]

Cooperative Institute for Mesoscale Meteorological Studies, University of Oklahoma, and NOAA/NWS/Warning Decision Training Division, Norman, Oklahoma

(Manuscript received 31 May 2016, in final form 25 October 2016)

ABSTRACT

Statistical evaluations of tornado warnings issued during recent tropical cyclone events yielded an above-average false alarm ratio. This study analyzed tornado-warned convection associated with Tropical Storms Debby (2012) and Andrea (2013) using superresolution and dual-polarization data from Weather Surveillance Radar-1988 Doppler radars located throughout the Florida peninsula to identify precursor characteristics and signatures that would distinguish tornadic events prior to tornadogenesis. A series of radar-based interrogation guidance at varying ranges from radar is presented to help facilitate the reduction of the tornado-warning false alarm ratio without compromising the probability of detection. For convection within 74.1 km from the nearest radar, low-level velocity characteristics include a rotational velocity $\geq 10.3\ \mathrm{m\ s^{-1}}$ (20 kt), shear across the rotation $\geq 0.010\ \mathrm{s^{-1}}$, and a contracting rotation diameter. The convection should also exhibit supercell reflectivity signatures and at least a mesocyclone velocity enhancement signature or horizontal separation of greater Z_{DR} and K_{DP} values. Guidance at a range from 74.1 to 129.6 km is similar except for not requiring the presence of a supercell reflectivity signature and the change of the rotational velocity guidance to $\geq 7.7\ \mathrm{m\ s^{-1}}$ (15 kt) at the 0.5°-elevation angle. Convection at a range beyond 129.6 km only requires a rotational velocity $\geq 7.7\ \mathrm{m\ s^{-1}}$ (15 kt) at the 0.5°-elevation angle. Evaluation of the radar interrogation guidance for tornadic events and tornado-warned convection for six tropical cyclones reduced the number of false alarm events by 28.9% and reduced the false alarm ratio from 0.740 to 0.669.

1. Introduction

An estimated 1800 tornadoes have been associated with tropical cyclones (TCs) from 1950 to 2007, which accounted for 3.4% of all tornadoes that occurred in the United States (Schultz and Cecil 2009). TC tornadoes are typically weak, and only 14% of them were rated F/EF2 or higher (Schultz and Cecil 2009). More than 20% of deadly U.S. TCs had at least one direct fatality from tornadoes, while only 3% of direct TC fatalities from 1963 to 2012 were attributable to tornadoes (Rappaport 2014). Although tornadoes are responsible for a small percentage of damage and direct casualties, the operational assessment and warning decision-making with respect to TC tornadoes are still a challenge.

The National Weather Service (NWS) performs a service assessment to evaluate its performance and the effectiveness of its products and services following a significant event. One finding from the assessment of Hurricane Irene (2011) discussed the above-average tornado warning (TOR) false alarm ratio (FAR) and its impact on local media coverage regarding other, more immediate TC hazards (NWS 2012). This FAR concern can be illustrated by plotting the average FAR for each TC event from 2008 to 2013 that produced at least one confirmed tornado with at least 10 TORs issued (Fig. 1). A total of 1397 tornado warnings were issued during these 12 TC events, of which 1199 tornado warnings did not verify. The TOR FAR for each event was greater than the 2013 NWS Government Performance Requirements Act (GPRA) FAR performance metric of 0.72. The average FAR of these events was 0.858.

Most TC tornadoes are produced by supercells. An evaluation of TC events from 2003 to 2011 determined

[a] Current affiliation: Cooperative Institute for Mesoscale Meteorological Studies, University of Oklahoma, and NOAA/OAR/National Severe Storms Laboratory, Norman, Oklahoma.

Corresponding author e-mail: Steven M. Martinaitis, steven.martinaitis@noaa.gov

DOI: 10.1175/WAF-D-16-0105.1

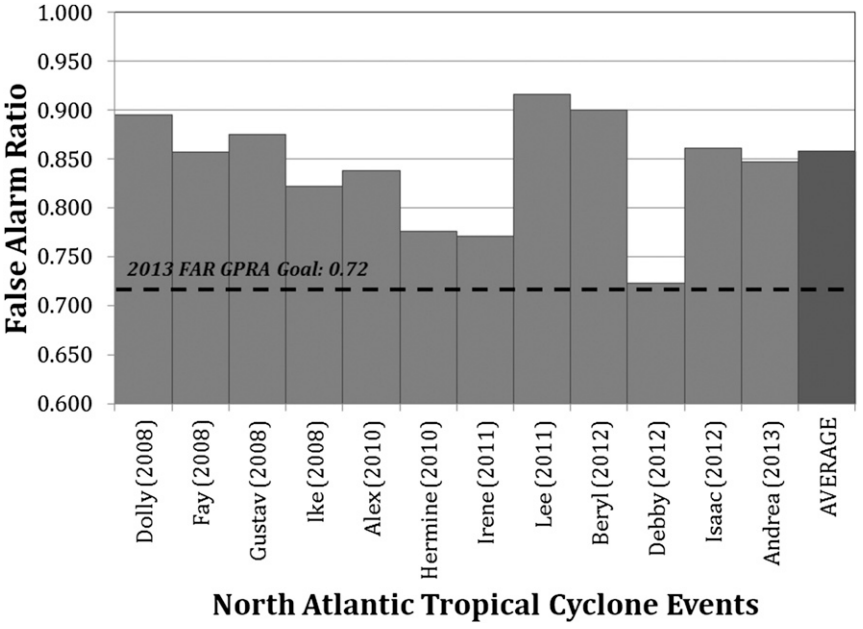

FIG. 1. TOR FAR for North Atlantic TC events from 2008 to 2013. Each TC event had at least 10 TORs issued with at least one confirmed tornado. The average TOR FAR is depicted in the far-right column of the graph. The dashed line represents the 2013 GPRA goal for TOR FAR.

that 88% of tornadoes and 100% of strong tornadoes (F/EF2 or higher) formed within supercell or marginal supercell storms (Edwards et al. 2012). Previous studies have evaluated observed reflectivity structures of tornado-producing convection associated with TC events using the Weather Surveillance Radar-1988 Doppler (WSR-88D) radar network. Tornadic storms had small, discrete reflectivity values above 50 dBZ that were more diminutive in size when compared with classic Great Plains supercells (e.g., Spratt et al. 1997; McCaul et al. 2004). Supercellular reflectivity features like appendages, hook echoes, forward-flank notches, weak-echo regions (WERs), and bounded weak-echo regions (BWERs) were not always apparent and often subtle (e.g., Spratt et al. 1997; Devanas et al. 2008). Hook echoes or appendage signatures were observed prior to tornadogenesis in 75% of the tornadic events evaluated by Schneider and Sharp (2007); however, it was noted that relying on such signatures alone would result in missed tornadic events. The majority of tornado-producing cells without identifiable supercell reflectivity signatures were observed at long ranges from the radar (Spratt et al. 1997; Schneider and Sharp 2007).

Numerous studies also interrogated various low-level velocity characteristics and trends of tornadic events. The rotational velocity V_r strength is generally a key variable for operational tornado-warning decision-making. Detailed velocity assessments of TC tornadoes by Spratt et al. (1997) identified rotation within convection an average of 30 min prior to tornado production with V_r values of 6.7–15.4 m s^{-1} (13–30 kt) near the time of tornadogenesis. The diameter of the low-level mesocyclone (i.e., the distance across the maximum inbound and outbound velocity values) was also found to be contracting over time, with some tornadic mesocyclones contracting to near 1.85 km (1.0 n mi). More recent studies confirmed the trend of a contracting diameter, while stating that most tornadic storms exhibited V_r values of at least 9.2–10.3 m s^{-1} (18–20 kt) just prior to tornadogenesis (McCaul et al. 2004; Schneider and Sharp 2007; Devanas et al. 2008). Low-level shears across the circulation have been observed to be at or above 0.010 s^{-1} for most tornadic events (e.g., Spratt et al. 1997; Schneider and Sharp 2007); however, shear values were frequently less than 0.010 s^{-1} with storms more than 80 km from a WSR-88D (McCaul et al. 2004).

While much attention has been given to the low-level rotational characteristics, Schneider and Sharp (2007) evaluated the midlevel velocity field for additional means of distinguishing storms with increased tornadic potential. Mesocyclones were rarely observed above the 1.5°-elevation angle and were described as broad areas of rotation, with inbound and outbound velocities separated by at least 5.5 km (3 n mi). Enhanced midlevel radial velocities of at least 15.4 m s^{-1} (30 kt) vertically collocated with a hook and low-level rotational signature were

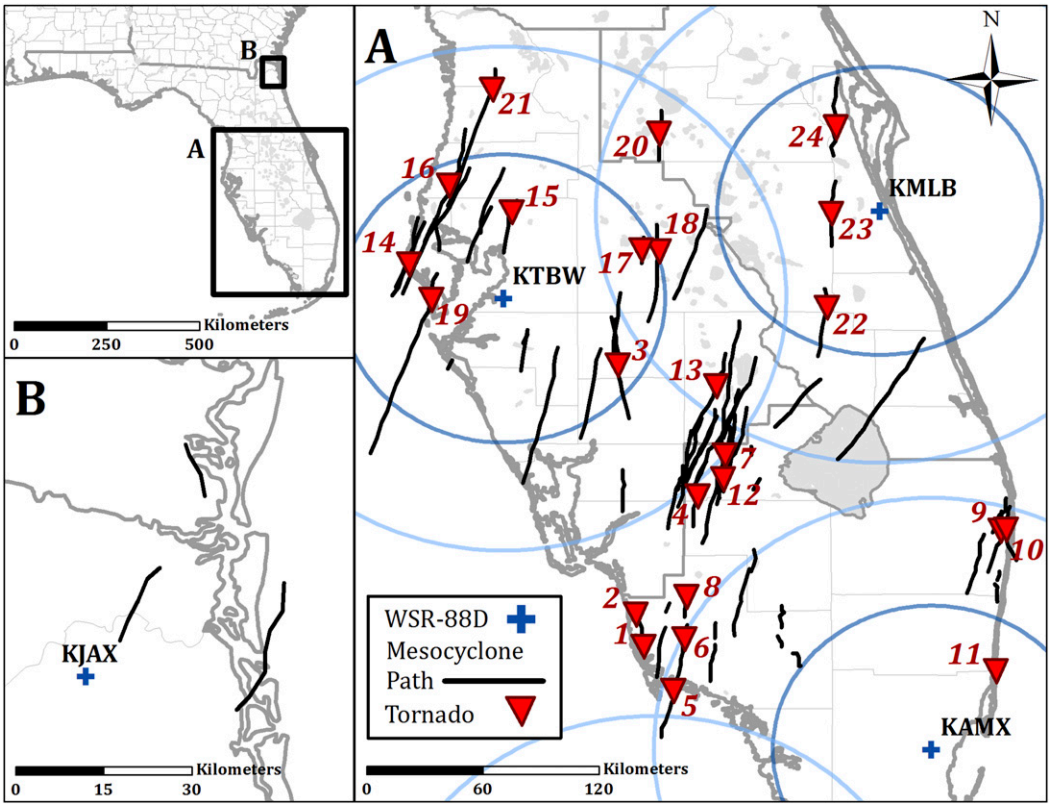

FIG. 2. Map of rotation tracks for all tornado-warned events during Tropical Storm Debby in areas covered by NWS WFOs in FL. Confirmed tornadoes represented by red triangles with the adjacent number corresponding to the tornado events detailed in Table 1. Locations of WSR-88D radars (blue crosses) with range rings of 74.1 km (40.0 n mi; blue circles) and 129.6 km (70.0 n mi; light-blue circles) are also shown. The WSR-88D radars displayed are as follows: Miami (KAMX), Jacksonville (KJAX), Melbourne (KMLB), and Tampa Bay (KTBW).

found in 14 of 15 tornadic storms analyzed by Schneider and Sharp (2007). Defined as a velocity enhancement signature (VES), this feature was observed between 2.1 km (7.0 kft) and 4.2 km (14.0 kft) above ground level (AGL) at an average of 27 min prior to tornadogenesis. While a VES could offer a high probability of tornadic development, the authors suggested that it could also yield a high false alarm percentage.

A dual-polarization assessment of tornado-warned storms with Hurricane Rita (2005) was conducted by Crowe et al. (2010) utilizing the Advanced Radar for Meteorological Operational Research (ARMOR) C-band radar in Huntsville, Alabama. Differential reflectivity Z_{DR} and specific differential phase K_{DP} values were compared between three different storms that traversed within 50 km of the ARMOR radar: one tornadic, one funnel producing, and one non–funnel producing. Analysis at 1 km AGL found a clear horizontal displacement of the maximum Z_{DR} and K_{DP} values and a Z_{DR} arc signature within the tornadic storm prior to tornadogenesis. Greater Z_{DR} values were located in the forward flank of the cell, downshear of the main updraft, while K_{DP} values maximized on the right-rear quadrant. This separation suggested drop size sorting of hydrometeors from increased directional shear due to strong mesocyclone development, as previously noted in Great Plains supercells (Kumjian and Ryzhkov 2008, 2009; Romine et al. 2008; Crowe et al. 2010). More recent work has noted the correlation of size sorting with off-hodograph motion of convection and associated storm-relative mean wind (Dawson et al. 2015).

There are many challenges with identifying tornadic events with TCs prior to tornadogenesis. A number of studies assessed tornadic storms within the context of establishing preliminary criteria and radar-derived precursors for operational warning decision-making and tornado detection (e.g., Spratt et al. 1997; Schneider and Sharp 2007; Devanas et al. 2008). Given the rapid strengthening and weakening of mesocyclones within TC convection, the entire life span of some tornadoes could occur between volume scans of the lowest elevation angles. Sampling of shallow rotational velocity

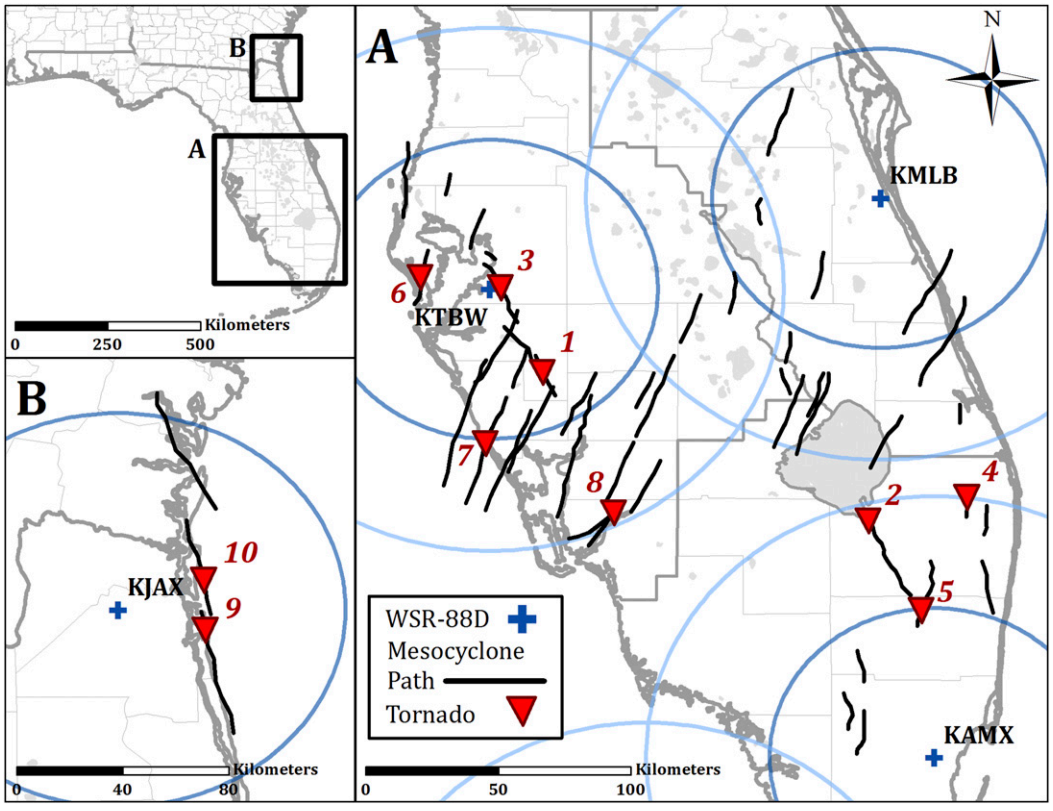

FIG. 3. As in Fig. 2, but for Tropical Storm Andrea. The numbers adjacent to the confirmed tornadoes correspond to the tornado events detailed in Table 2.

signatures at farther ranges from the radar were physically limited by the "aspect ratio" and "radar horizon" of the WSR-88D (Burgess et al. 1993; Spratt et al. 1997). Supercell reflectivity signatures were also more challenging to detect at longer ranges from radar.

The aforementioned studies that utilized WSR-88D radars were conducted prior to two significant technological upgrades. An enhancement in the spatial resolution of base data, which is referred to as superresolution, was implemented in 2008 (Torres and Curtis 2007). This superresolution upgrade increased the legacy reflectivity grid spacing of 1 km in range and 1.0° in azimuth and the legacy velocity grid spacing of 250 m in range and 1.0° in azimuth to a grid spacing of 250 m in range to 0.5° in azimuth. Dual-polarization technology, which allows a radar to send both vertical and horizontal polarized signals to provide more information about atmospheric features, was fully implemented by 2013 (Leifer et al. 2013). The goal of this study is to build upon previous findings on radar-based tornadogenesis precursors in TC convection to reduce the above-average TOR FAR using the updated WSR-88D radar network. The study assessed tornado-warned convection associated with Tropical Storms Debby (2012) and Andrea (2013) over the Florida peninsula. Storm-scale radar characteristics and temporal trends were statistically evaluated to identify means of discriminating tornadic storms from their nontornadic counterparts and to define a set of radar interrogation guidance that can be beneficial to the operational warning decision-making process.

2. Methodology

Archived WSR-88D radar data of Tropical Storms Debby and Andrea were reviewed using the Weather Event Simulator (WES), a data playback and simulation platform in the Advanced Weather Interactive Processing System (AWIPS) software (e.g., Magsig and Page 2002; Magsig et al. 2004, 2006). The archived data were localized to the following NWS Weather Forecast Offices (WFOs) in Florida: Jacksonville (JAX), Melbourne (MLB), Miami (MFL), and Tampa Bay (TBW). A total of 76 tornado-warned circulations over land were identified with Tropical Storm Debby during 23–25 June 2012 (Fig. 2). A total of 48 tornado-warned circulations were identified with Tropical Storm Andrea on 6 June 2013 (Fig. 3). Other strong circulations

TABLE 1. List of tornado events over FL during Tropical Storm Debby, 23–25 Jun 2012, in chronological order. Listed in this table are the date and time (UTC) of tornadogenesis; the city nearest to the tornado path; the duration, length, width, and rating of the tornado; and the range from the nearest WSR-88D at time of tornadogenesis. Data about these tornadic events were provided by NWS *Storm Data* through the NWS Performance Management System (https://verification.nws.noaa.gov/). The time of tornadogenesis and pathlength of event 5 was classified based on its origin as a waterspout prior to moving onshore. The radar-based estimated time of event 5 moving onshore was 1527 UTC.

Event No.	Time and date	Location	Duration (min)	Length (km)	Width (m)	Rating	Range (km)
1	1935 UTC 23 Jun	East Naples	2	2.7	18	EF0	144
2	2000 UTC 23 Jun	Naples Park	<1	0.1	9	EF0	154
3	1415 UTC 24 Jun	Buchanan	15	27.4	91	EF0	61
4	1500 UTC 24 Jun	Muse	<1	<0.1	9	EF0	133
5	1510 UTC 24 Jun	Goodland	30	26.1	27	EF0	124
6	1600 UTC 24 Jun	Golden Gate	<1	<0.1	18	EF0	128
7	1623 UTC 24 Jun	Venus	6	5.6	137	EF0	130
8	1625 UTC 24 Jun	Corkscrew	2	0.2	18	EF0	139
9	1625 UTC 24 Jun	Lake Worth	<1	<0.1	18	EF0	119
10	1725 UTC 24 Jun	Westgate	2	1.9	27	EF0	120
11	1805 UTC 24 Jun	Golden Beach	1	0.8	18	EF0	52
12	1904 UTC 24 Jun	Palmdale	<1	<0.1	18	EF0	170
13	1923 UTC 24 Jun	Lake Placid	7	8.5	91	EF1	107
14	1940 UTC 24 Jun	Indian Rocks Beach	3	1.2	69	EF1	46
15	2039 UTC 24 Jun	Lutz	2	1.7	46	EF0	46
16	2117 UTC 24 Jun	New Port Richey	2	0.6	69	EF1	65
17	2255 UTC 24 Jun	Winter Haven	1	1.5	23	EF0	69
18	0004 UTC 25 Jun	Winter Haven	8	10.0	137	EF2	76
19	0021 UTC 25 Jun	St. Pete Beach	4	4.9	46	EF1	33
20	0059 UTC 25 Jun	Winter Garden	6	6.0	91	EF0	107
21	0127 UTC 25 Jun	Homosassa Springs	6	8.0	91	EF1	109
22	0155 UTC 25 Jun	Yeehaw Junction	7	5.0	91	EF0	56
23	0246 UTC 25 Jun	Deer Park	1	1.9	46	EF0	22
24	0337 UTC 25 Jun	W of Titusville	1	1.9	23	EF0	48

existed offshore; however, these were not considered because of a lack of verification. Table 1 lists the 24 confirmed tornadoes verified by ground surveys from Tropical Storm Debby. Table 2 provides the same information for the 10 verified tornadoes from Tropical Storm Andrea. Only 1 of the 34 tornadic circulations evaluated in this study produced a tornado that was rated greater than EF1 (event 18 in Table 1, an EF2). Ten of the tornadoes lasted more than 5 min, of which four existed more than 10 min. Most of the tornadoes were also small in size, with all but three tornadoes having an estimated maximum width of less than 100 m.

Comparative assessments of several TC tornadic precursors were conducted during the life cycle of each circulation. The median life cycle for low-level circulations was approximately 40 min for tornadic convection and 30 min for nontornadic convection. The examination of low-level features were conducted at the 0.5°- and 1.5°-elevation angles, since these tilts are present with all employed WSR-88D volume coverage patterns (VCPs;

TABLE 2. As in Table 1, but for Tropical Storm Andrea on 6 Jun 2013. Data related to these tornadic events were provided by NWS *Storm Data* through the NWS Performance Management System (https://verification.nws.noaa.gov/).

Event No.	Time and date	Location	Duration (min)	Length (km)	Width (m)	Rating	Range (km)
1	0649 UTC 6 Jun	Myakka City	2	2.1	46	EF0	46
2	0718 UTC 6 Jun	Belle Glade	2	1.2	23	EF0	120
3	0747 UTC 6 Jun	Sun City Center	4	4.4	46	EF0	6
4	1045 UTC 6 Jun	Royal Palm Beach	5	3.7	91	EF1	130
5	1205 UTC 6 Jun	Coral Springs	30	26.8	23	EF0	70
6	1403 UTC 6 Jun	Gulfport	2	3.5	46	EF0	31
7	1513 UTC 6 Jun	South Venice	3	3.0	46	EF0	80
8	1805 UTC 6 Jun	Fort Myers Shores	2	0.5	27	EF0	122
9	2048 UTC 6 Jun	Fernandina Beach	24	35.0	644	EF1	30
10	2107 UTC 6 Jun	Suwannee Springs	3	5.9	91	EF0	30

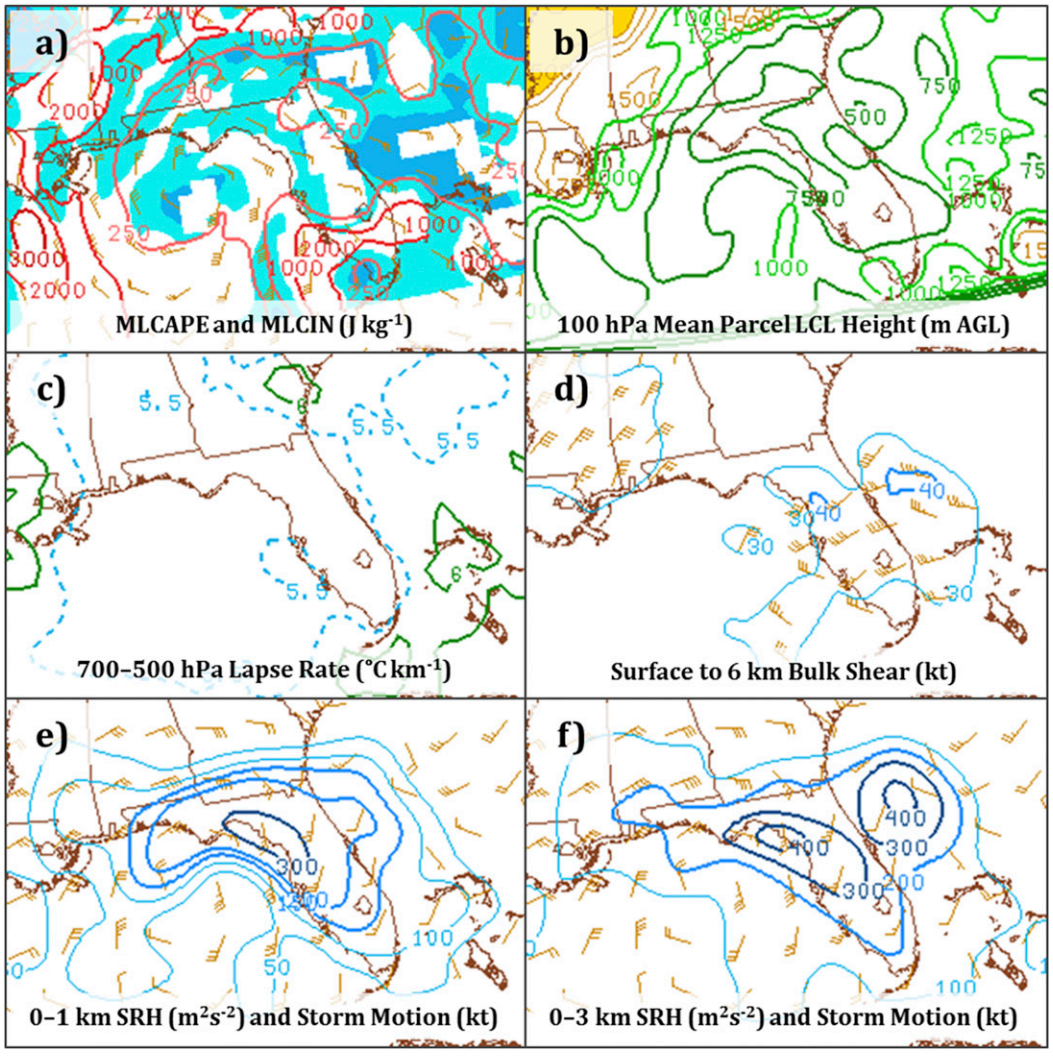

FIG. 4. SPC mesoscale analysis during Tropical Storm Debby at 0000 UTC 25 Jun 2012 for the following environmental parameters: (a) MLCAPE (contours) and mixed layer convective inhibition (MLCIN; shaded; J kg^{-1}), (b) 100-hPa mean parcel lifting condensation level (LCL) height (m AGL), (c) 700–500-hPa lapse rate (°C km^{-1}), (d) surface–6-km bulk shear (barbs and contours; kt), (e) 0–1-km SRH (contours; m^2 s^{-2})and storm motion (barbs; kt), and (f) 0–3-km SRH (contours; m^2 s^{-2}) and storm motion (barbs; kt). MLCIN in (a) is shaded light blue for values of 25–100 J kg^{-1} and blue for values > 100 J kg^{-1}. The storm motion in (e) and (f) is estimated using Bunkers et al. (2000). Data were obtained from the SPC's mesoscale analysis pages (http://www.spc.noaa.gov/exper/mesoanalysis/).

e.g., Crum et al. 1993; Brown et al. 2005). Sampling limitations, such as ground clutter, velocity range folding, and the cone of silence, limited the analysis of some events. The WSR-88D radars utilized various VCPs during Tropical Storms Debby and Andrea. The completion time of a volume scan can range from 270 to 360 s for VCPs designed for precipitation events; thus, the assessment of temporal trends was conducted based on the number of volume scans from tornadogenesis or maximum rotational intensity based on low-level shear values for nontornadic storms. Analysis of reflectivity and velocity trends focused on the period from the volume scan (VS) containing tornadogenesis or time of maximum rotational intensity for nontornadic storms (VS = 0) to three volume scans prior (VS = −3). Similar patterns were seen in the analysis of both the 0.5°- and 1.5°-elevation angles for both reflectivity and velocity assessments; thus, statistical and temporal evaluations are presented in this study at the 0.5°-elevation angle only.

Velocity characteristics examined include low-level V_r, the diameter of the rotation feature, and the shear across the rotation feature. Low-level rotation for this

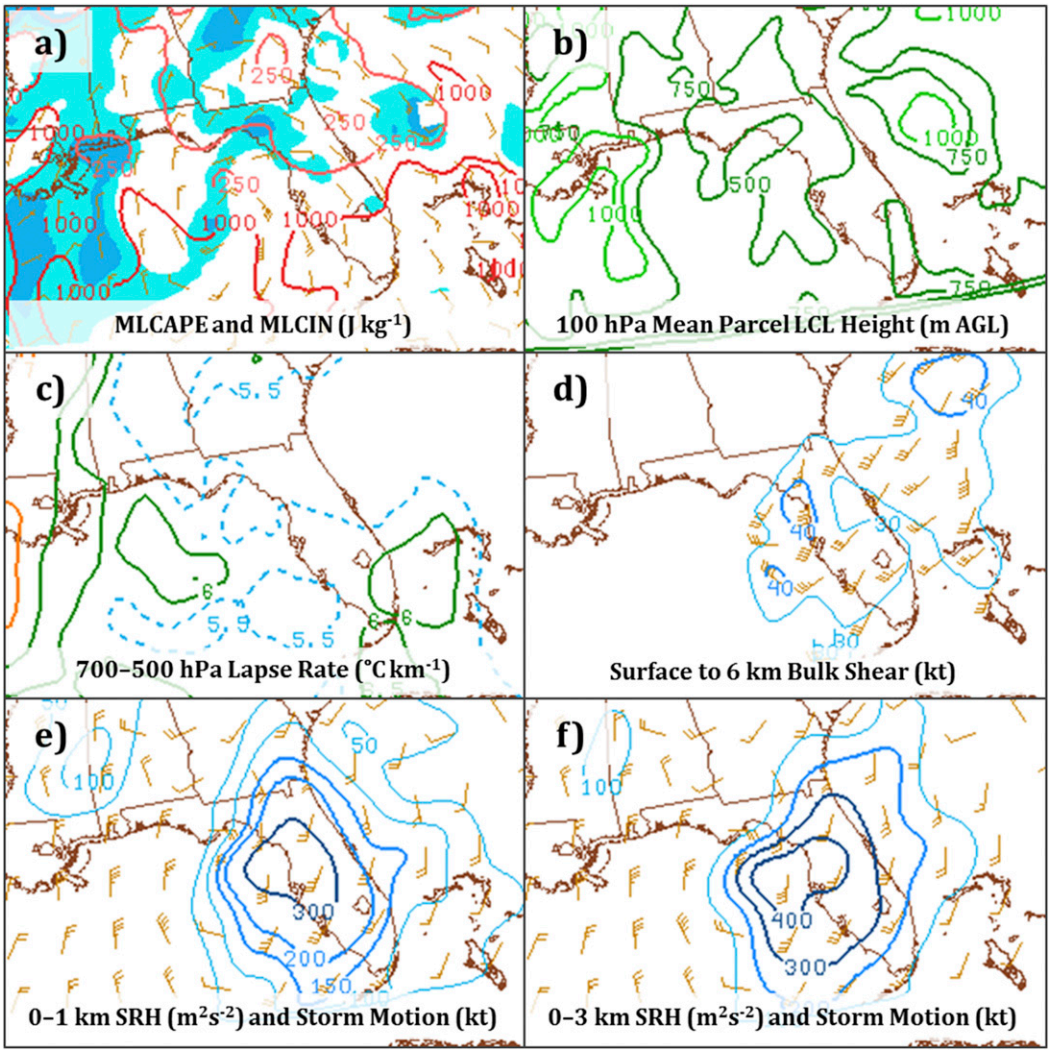

FIG. 5. As in Fig. 4, but during Tropical Storm Andrea at 1500 UTC 6 Jun 2013.

study were defined as having a V_r of at least 4.1 m s^{-1} (8 kt) and a diameter of less than 6 km at the 0.5°-elevation angle. The diameter of the rotation feature is defined as the distance between the maximum velocity V_{max} and minimum velocity V_{min}. It is important to note that although mesocyclones are a three-dimensional velocity feature, rotation with distant convection might only be sampled by the lowest elevation angle; thus, rotation identified at only a single elevation angle will be defined as a two-dimensional circulation because of the lack of radar-based vertical continuity. All available elevation angles of velocity data were also examined for the presence of enhanced radial velocities above the low-level circulation. Sampling limitations, shallow convection, and fast storm motion created challenges with identifying WERs and BWERs; thus, analyses of these features were not considered in this study.

The subjective reflectivity assessment included the identification of supercell characteristics, such as inflow notches, hook echoes, or appendages. The horizontal separation of maximum Z_{DR} and K_{DP} values was evaluated at the 0.5°-elevation angle. The values and temporal trends for reflectivity, vertically integrated liquid (VIL), and spectrum width (SW) were also evaluated. All tornado-warned events had reflectivity values $\geq$ 50 dBZ regardless of tornadic potential, and there were significant storm-to-storm variabilities of VIL and SW values. The analysis yielded no distinguishing measures between tornadic and nontornadic events for these products; thus, results for these product values were not presented in this study.

A set of radar interrogation guidance was derived from the resulting evaluations. Each event from Tropical Storms Debby and Andrea was then reexamined using the radar-interrogated guidance. An independent

dataset of four other TC events with tornadic activity during the WSR-88D dual-polarization era was also evaluated. A binary yes/no decision regarding the issuance of a TOR was made for each storm, given the assumption that only one circulation is included in each warning decision. Storm-based warning performance metrics for POD and FAR were then established pre- and postimplementation of the radar interrogation guidance.

3. Synoptic overview

a. Debby (2012)

Tropical Storm Debby was first classified at 1200 UTC 23 June 2012, approximately 355 km south-southeast of the mouth of the Mississippi River. Tropical Storm Debby tracked to the north-northeast and then accelerated to the east-northeast on 26 June 2012. The TC made landfall near Steinhatchee, Florida, at 2100 UTC 26 June. Maximum sustained winds at landfall were estimated at 18.0 m s^{-1}, and the estimated minimum central pressure was 995 hPa. For a complete discussion of Tropical Storm Debby, see Kimberlain (2013). Tornadic activity over Florida occurred more than 40 h prior to landfall. The first two tornadoes occurred between 1930 and 2000 UTC 23 June, while the rest of the tornadic activity developed between 1400 UTC 24 June and 0400 UTC 25 June. All tornadic activity over Florida was confined to the southern two-thirds of the Florida peninsula (Fig. 2). Nineteen of the 24 tornadoes were located in the right-front quadrant of Debby between 50° and 90° azimuth with respect to TC motion. The other five tornados were located in the right-rear quadrant between 90° and 105°. The mean radius of tornadoes occurring from the center of Debby was 466 km.

Tornadic storms were generally isolated cells while some tornadic activity was along convective bands associated with the TC. Mesoscale analysis from the Storm Prediction Center (SPC) at 0000 UTC 25 June depicted modest instability with less than 250 J kg^{-1} mixed layer convective available potential energy (MLCAPE) in the northern part of the Florida peninsula and over 1000 J kg^{-1} MLCAPE in southern Florida (Fig. 4a); however, the northward extension of greater MLCAPE values was collocated with regions of midlevel dry air being entrained into the TC, which has been shown to enhance the surface-based instability and evaporative cooling (Vescio et al. 1996; Curtis 2004). Lifting condensation level heights were generally less than 750 m AGL (Fig. 4b) with a 700–500-hPa lapse rate around 5.5°C km^{-1} (Fig. 4c). The shear profile was favorable for tornadic activity within TCs (Edwards et al. 2012). The surface–6-km bulk shear was over 15.4 m s^{-1} (30 kt)

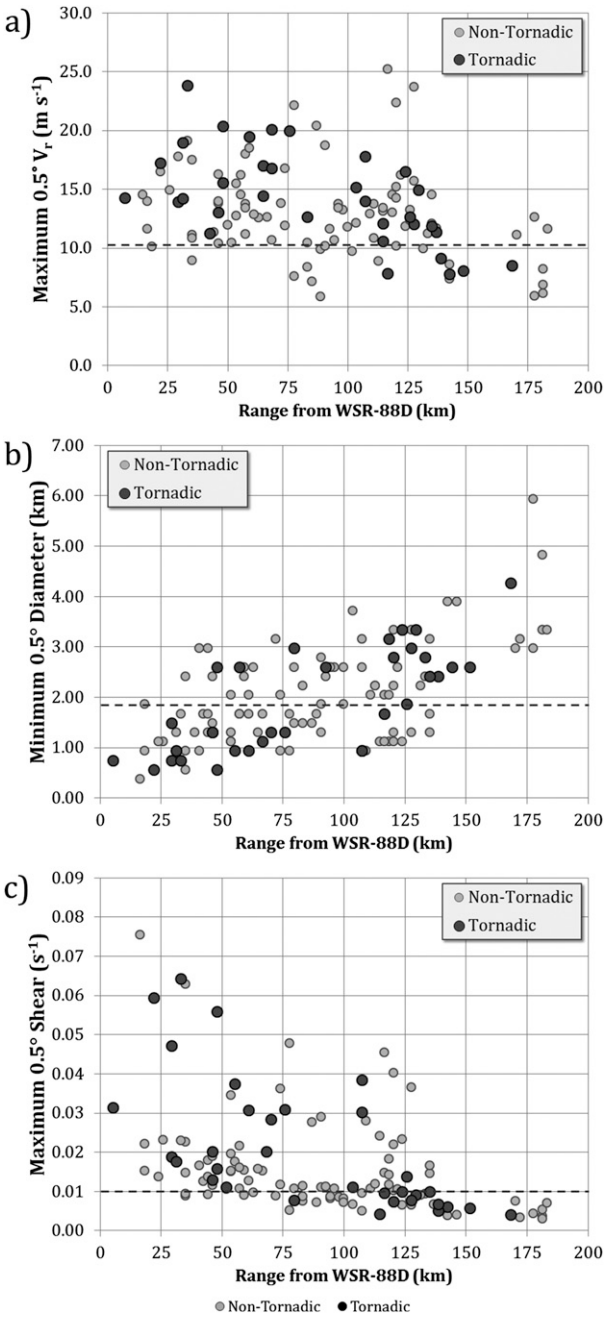

FIG. 6. Scatterplots of (a) maximum V_r, (b) minimum diameter, and (c) maximum shear across the rotation at an 0.5°-elevation angle with respect to range from the nearest WSR-88D radar. Tornadic events are represented by dark gray circles, and nontornadic events are represented by light-gray circles. The values plotted are the peak values for each velocity characteristic at any time between VS = −3 and 0. The dashed line in each scatterplot represents the following: in (a) the threshold of V_r = 10.3 m s^{-1} (20 kt) based on findings from Schneider and Sharp (2007), in (b) the threshold of diameter = 1.85 km (1.0 n mi) based on findings from Spratt et al. (1997), and in (c) the threshold of shear = 0.010 s^{-1} based on findings from Spratt et al. (1997).

TABLE 3. Statistical evaluation of velocity characteristic peak values for tornadic and nontornadic events occurring <74.1 km (40 n mi) from the nearest radar. Low-level velocity characteristics listed are the V_r (m s^{-1}), diameter (km), and shear across the rotation (s^{-1}) at the 0.5°-elevation angle. Statistics listed are the sample size N, median, mean μ, standard deviation σ, the p value from two-sample t tests assuming equal variances, and Levene's test for the equality of variances results. A p value ≤ 0.05 signifies a significant statistical difference between the tornadic and nontornadic values.

	V_r (m s^{-1})		Diameter (km)		Shear (s^{-1})	
	Nontornadic	Tornadic	Nontornadic	Tornadic	Nontornadic	Tornadic
N	34	15	34	15	34	15
Median	13.75	16.72	1.67	0.93	0.0152	0.0282
μ	13.85	16.65	1.70	1.19	0.0187	0.0313
σ	2.89	3.36	0.71	0.64	0.0140	0.0176
t test	$p = 0.005$		$p = 0.020$		$p = 0.010$	
Levene's test	$F = 0.464$, $p = 0.499$		$F = 0.371$, $p = 0.546$		$F = 3.461$, $p = 0.069$	

across most of the Florida peninsula (Fig. 4d), while both 0–1-km and 0–3-km storm-relative helicity (SRH), the measure of potential cyclonic updraft rotation in right-moving supercells, was over 200 m^2 s^{-2} (Figs. 4e–f).

b. Andrea (2013)

Tropical Storm Andrea was first classified at 1800 UTC 5 June 2013 approximately 500 km southwest of St. Petersburg, Florida. After slowly moving northward on 5 June, Tropical Storm Andrea accelerated to the northeast and made landfall along the northwestern coast of the Florida peninsula at 2200 UTC 6 June. Maximum sustained winds were estimated at 25.7 m s^{-1}, and the estimated minimum central pressure was 992 hPa. For a complete discussion of Tropical Storm Andrea, see Beven (2013). Tornadic activity over Florida occurred prior to landfall between 0630 and 2130 UTC 6 June. Of the 10 confirmed tornadoes, 8 occurred in the southeast and west-central portions of the Florida peninsula, while the other 2 occurred in the far northeast corner of the state (Fig. 3). Nine of the 10 tornadoes were located in the right-front quadrant of Andrea between 20° and 90° azimuth with respect to TC motion. The 10th tornado was located in the right-rear quadrant at an azimuth of approximately 115°. The mean radius of tornadoes occurring from the center of Andrea was 331 km.

Tornadic development occurred along convective bands collocated with regions of midlevel dry air within an environment similar to that analyzed during Tropical Storm Debby. Mesoscale analysis from SPC at 1500 UTC 6 June showed modest instability with less than 250 J kg^{-1} MLCAPE in the northern half of the Florida peninsula and over 1000 J kg^{-1} MLCAPE south of Lake Okeechobee (Fig. 5a); however, the slight northward extension of greater MLCAPE values was collocated with regions of midlevel dry air being entrained into the TC. Forecast Rapid Refresh (RAP) model soundings (not shown) were able to depict the dry-air entrainment and its resulting increased surface heating and instability ahead of the convective bands. Lifting condensation level heights were generally between 500 and 750 m AGL (Fig. 5b) with a 700–500-hPa lapse rate around 5.5°–6.0°C km^{-1} (Fig. 5c). Despite the varying degrees of instability, the low-level shear profiles were favorable for tornadic development (Edwards et al. 2012). The surface–6-km bulk shear was over 15.4 m s^{-1} (30 kt) across most of the Florida peninsula (Fig. 5d), while both the 0–1- and 0–3-km SRH values were over 300 m^2 s^{-2} (Figs. 5e–f).

4. Analysis of storm-scale features

a. Low-level velocity characteristics

All tornadic events and tornado-warned nontornadic events were assessed from VS = −3 through VS = 0, and

TABLE 4. As in Table 3, but for tornadic and nontornadic events occurring ≥74.1 km (40 n mi) from the nearest radar.

	V_r (m s^{-1})		Diameter (km)		Shear (s^{-1})	
	Nontornadic	Tornadic	Nontornadic	Tornadic	Nontornadic	Tornadic
N	53	18	53	18	53	18
Median	11.86	12.03	2.22	2.59	0.0102	0.0083
μ	12.51	12.34	2.31	2.49	0.0137	0.0120
σ	4.38	3.53	1.03	0.88	0.0110	0.0101
t test	$p = 0.878$		$p = 0.518$		$p = 0.551$	
Levene's test	$F = 0.322$, $p = 0.572$		$F = 0.656$, $p = 0.421$		$F = 0.267$, $p = 0.607$	

the peak values for each velocity characteristic at any time between VS = −3 and 0 were plotted against their distance from the nearest radar (Fig. 6). Notable patterns of peak velocity characteristic versus distance were apparent. Maximum observed $V_r > 10.3\,\mathrm{m\,s^{-1}}$ (20 kt) were found in 28 of the 33 tornadic events shown in Fig. 6a. The five tornadic events that had observed $V_r < 10.3\,\mathrm{m\,s^{-1}}$ were >115 km from the nearest radar. A total of 13 tornadic circulations within 74.1 km (40 n mi) of the nearest radar had a minimum observed diameter ranging from 0.56 km (0.3 n mi) to 1.48 km (0.8 n mi) at the 0.5°-elevation angle (Fig. 6b); however, the diameter of two tornadic circulations in this range only contracted to 2.60 km (1.4 n mi). In contrast, the minimum diameter for 13 of the 18 of tornadic events beyond 74.1 km from the nearest radar was greater than 1.85 km and ranged from 2.41 km (1.3 n mi) to 4.26 km (2.3 n mi). Maximum shear values for all tornadic events within 74.1 km of the nearest radar were at least $0.010\,\mathrm{s^{-1}}$ (Fig. 6c). Four tornadic events had shear across the rotation exceeding $0.040\,\mathrm{s^{-1}}$ at the VS containing tornadogenesis (VS = 0). The maximum shear values for 13 of the 18 tornadic events at a range ≥ 74.1 km were $<0.010\,\mathrm{s^{-1}}$. Similar patterns for nontornadic events were seen in the distribution of peak values versus the range from radar for all three velocity characteristics studied.

A statistical evaluation of the peak velocity characteristic values was conducted between tornadic and nontornadic events. The events were delineated using an arbitrary distance threshold of 74.1 km (40 n mi) from the nearest radar. Table 3 displays the statistics for events within 74.1 km. The maximum V_r for tornadic events were approximately $3\,\mathrm{m\,s^{-1}}$ stronger than for the tornado-warned nontornadic events. Noticeable differences in the median and mean values were also present with minimum diameter size and shear across the circulation. A two-sample t test assuming equal variances and Levene's test for equality of variances (Levene 1960) were conducted for each velocity characteristic between tornadic and nontornadic events. An alpha α threshold of 0.05 was established to determine if there were statistically significant differences. The two-sample t tests concluded that all velocity characteristics differences between tornadic and nontornadic events at a range of <74.1 km were statistically significant (i.e., p values ≤ 0.05). In contrast, no significant statistical differences were found for all velocity characteristics with events occurring ≥ 74.1 km from the nearest radar (Table 4), which means that it can be particularly challenging to use velocity characteristics to identify potentially tornadic events. The group variances for each velocity characteristic for both ranges from radar can be treated as equal (i.e., not statistically significant).

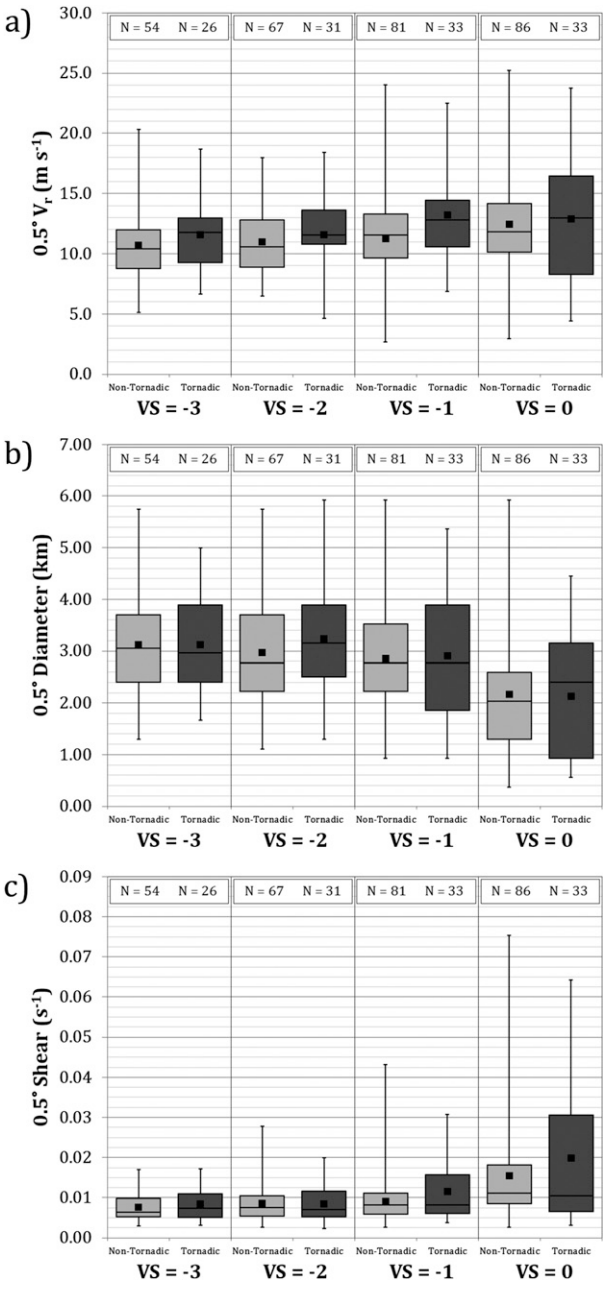

FIG. 7. Box-and-whisker plot of (a) V_r, (b) diameter size, and (c) shear across the rotation at the 0.5°-elevation angle for tornadic (dark gray) and nontornadic (light gray) events from VS = −3 to 0. The top (bottom) of each box represents the 75th (25th) percentile with the line in the middle of each box representing the median value. The top (bottom) whisker represents the maximum (minimum) value observed. The mean value is represented by the point overlaid on top of each box-and-whisker plot. The sample size N is denoted at the top of each column.

The temporal trends for each velocity characteristic at the 0.5°-elevation angle are depicted in Fig. 7. The overall trend of V_r values of tornadic events increased through VS = −1 followed by a considerable spread in

TABLE 5. Statistical evaluation of V_r (m s^{-1}) from VS = −3 to 0 of both tornadic and nontornadic rotations at the 0.5°-elevation angle. Listed are the sample size N, median, mean μ, and standard deviation σ of V_r. Also listed are the p values from two-sample t tests assuming equal variances and Levene's test for the equality of variances results comparing the tornadic and nontornadic events at each VS. A p value ≤ 0.05 signifies that there was a significant difference between the tornadic and nontornadic V_r values at that VS.

	VS = −3		VS = −2		VS = −1		VS = 0	
	Nontornadic	Tornadic	Nontornadic	Tornadic	Nontornadic	Tornadic	Nontornadic	Tornadic
N	54	26	67	31	81	33	86	33
Median (m s^{-1})	10.39	11.76	10.57	11.55	11.57	12.81	11.85	12.99
μ (m s^{-1})	10.74	11.55	10.98	11.59	11.25	13.23	12.45	12.87
σ (m s^{-1})	2.86	3.23	2.68	2.91	3.30	4.03	4.16	4.65
t test	$p = 0.254$		$p = 0.310$		$p = 0.007$		$p = 0.632$	
Levene's test	$F = 0.294$, $p = 0589$		$F = 0.003$, $p = 0.954$		$F = 2.303$, $p = 0.132$		$F = 1.985$, $p = 0.162$	

V_r values at VS = 0 (Fig. 7a). Some values of V_r decreased prior to tornadogenesis. Approximately 45% of tornadic circulations had their maximum V_r value occur at VS = −1, while maximum V_r values were observed in 33% of tornadic circulations at VS = 0. While some V_r values observed by radar decreased prior to tornadogenesis, the contraction of the circulation diameter would increase the low-level shear values at the time of tornadogenesis. The overall trend for V_r values for nontornadic events increased steadily from VS = −3 to 0. The diameters of the rotation for both tornadic and nontornadic events were similar from VS = −3 to −2, followed by a contraction of the diameter to time VS = 0 (Fig. 7b). Analysis of the shear values also showed consistent values from VS = −3 to −2, followed by an increase in shear to VS = 0 (Fig. 7c). Considerable overlap of the box-and-whisker plots exists for all velocity characteristics between tornadic and nontornadic events; thus, identifying any temporal trends would be challenging in real time.

Statistical evaluations for V_r at each VS for tornadic and nontornadic events are displayed in Table 5. Similar statistics are shown for the diameter size (Table 6) and the shear across the rotation (Table 7). When comparing tornadic events against nontornadic events at each VS, the only statistically significant difference derived through the two-sample t tests assuming equal variances was with V_r values at VS = −1 (Table 5). This can be contributed to the 45% of tornadic storms that had V_r values peak at this time. The two-sample t-test p values at all other times and the other velocity characteristics suggest that differences were more likely due to chance. The group variances for each velocity characteristic were statistically significant (i.e., the group variances were unequal and the assumption of homogeneity of variances was violated) for the comparison of the rotation diameter at VS = 0 (Table 6) and the shear across the rotation at all evaluated times except for VS = −2 (Table 7) for tornadic versus nontornadic events.

The greatest change with velocity characteristics occurred between VS = −2 and the volume scans containing tornadogenesis or maximum intensity for nontornadic events, as seen in Fig. 6 and Tables 5–7. Additional analysis was conducted to determine if the trends in velocity characteristics were significantly different between tornadic and nontornadic events. Table 8 shows the rate of change from VS = −2 to the peak value normalized to the rate per VS for each velocity characteristic at a range < 74.1 km from the nearest radar. The rate of increase for V_r and shear with tornadic events was more than double the rate of increase for nontornadic events. The rate of contraction for the diameter per VS was greater for tornadic events but was only an average of 16% more than with nontornadic events. Two-sample t tests show that the trends in V_r and shear for tornadic events had a

TABLE 6. As in Table 5, but for the diameter (km) of the rotation at the 0.5°-elevation angle.

	VS = −3		VS = −2		VS = −1		VS = 0	
	Nontornadic	Tornadic	Nontornadic	Tornadic	Nontornadic	Tornadic	Nontornadic	Tornadic
N	54	26	67	31	81	33	86	33
Median (km)	3.06	2.96	2.78	3.15	2.78	2.78	2.04	2.41
μ (km)	3.12	3.12	2.98	3.23	2.85	2.90	2.16	2.13
σ (km)	0.99	0.98	1.09	1.11	1.04	1.14	1.05	1.17
t test	$p = 0.996$		$p = 0.277$		$p = 0.820$		$p = 0.887$	
Levene's test	$F = 0.168$, $p = 0.683$		$F = 0.014$, $p = 0.907$		$F = 1.488$, $p = 0.225$		$F = 4.846$, $p = 0.030$	

TABLE 7. As in Table 5, but for shear across the rotation (s^{-1}) at the 0.5°-elevation angle.

	VS = −3		VS = −2		VS = −1		VS = 0	
	Nontornadic	Tornadic	Nontornadic	Tornadic	Nontornadic	Tornadic	Nontornadic	Tornadic
N	54	26	67	31	81	33	86	33
Median (s^{-1})	0.0064	0.0073	0.0075	0.0070	0.0082	0.0081	0.0111	0.0105
μ (s^{-1})	0.0076	0.0085	0.0085	0.0084	0.0091	0.0115	0.0155	0.0198
σ (s^{-1})	0.0032	0.0042	0.0043	0.0044	0.0052	0.0075	0.0126	0.0175
t test	$p = 0.275$		$p = 0.884$		$p = 0.054$		$p = 0.137$	
Levene's test	$F = 6.822$, $p = 0.011$		$F = 0.726$, $p = 0.396$		$F = 11.467$, $p = 0.001$		$F = 8.805$, $p = 0.004$	

statistically significant difference from the nontornadic events, while there was no statistical significance between the tornadic and nontornadic rates of diameter contraction. Levene's test for the equality of variations also found statistically significant group variances for the trends of V_r and shear values. Evaluation of events occurring at a range ≥ 74.1 km from the nearest radar found smaller differences between tornadic and nontornadic events, which were confirmed by the high p values from the two-sample t tests and Levene's tests (Table 9).

b. *Midlevel velocity characteristics*

Assessment of midlevel velocity fields with each storm, especially in the range of 2.1–4.2 km (7.0–14.0 kft) AGL, found strong enhanced storm-relative radial velocities of 15.4 m s^{-1} (30 kt) that were collocated with the low-level rotation signature in tornadic and nontornadic convection. Schneider and Sharp (2007) defined these regions of collocated enhanced radial velocities as a velocity enhancement signature. It was hypothesized by Schneider and Sharp (2007) that a VES is a storm-scale inflow jet that influences the development or intensification of the rear-flank downdraft; however, similar radial velocity signatures were previously observed in studies regarding Great Plains supercells. Brandes (1977, 1978, 1984) observed highly asymmetric storm-relative rotation with the supercell mesocyclone around and above 3 km AGL with the strongest velocities on the right side of the storm with respect to deep-layer shear. The asymmetry between the inbound and outbound velocities has also been noted in model simulations of supercell thunderstorms where the three-dimensional mesocyclone structure was influenced by vertical pressure gradient forces and the nonuniform distribution of vertical vorticity (e.g., Rotunno 1984; Rotunno and Klemp 1985; Desrochers and Harris 1996). Midlevel mesocyclone asymmetries were also found to be influenced by nonlinear, off-hodograph motion deviating from mean flow (e.g., Rotunno and Klemp 1982; Weisman and Klemp 1984; Nolan 2004).

It can be hypothesized that a VES is the detection of the midlevel mesocyclone. Consider a supercell velocity field within a storm-relative framework (Fig. 8). When a storm is moving with the mean flow (i.e., on the hodograph), the storm-relative flow V_{SR} at the mean wind level is zero, and the rotation will appear to be nearly symmetric when viewing storm-relative velocity (SRM) values (Fig. 8a). A storm motion V_{storm} deviating off of the hodograph would generate a nonzero V_{SR} (Fig. 8b). When V_{SR} is superimposed on the vortex, the rotation will appear to be asymmetric, with the strongest SRM values on the right (inflow) side of the rotation. The velocity feature in question will hereinafter be referred

TABLE 8. Statistical evaluation of the change in velocity characteristics between VS = −2 and the peak value (occurring at either VS = −1 or 0) for tornadic and nontornadic events within 74.1 km (40 n mi) of the nearest radar. The rate of change shown is normalized to the rate of change per VS. Low-level velocity characteristics listed are the change in V_r (m s^{-1}), diameter (km), and shear across the rotation (s^{-1}) at the 0.5°-elevation angle. Statistics listed are the sample size N, median, mean μ, standard deviation σ, the p value from the two-sample t test assuming equal variances, and Levene's test for the equality of variances results. A p value ≤ 0.05 signifies significant statistical difference between the tornadic and nontornadic values.

	V_r (m s^{-1})		Diameter (km)		Shear (s^{-1})	
	Nontornadic	Tornadic	Nontornadic	Tornadic	Nontornadic	Tornadic
N	27	13	27	13	27	13
Median	+2.00	+3.75	−0.56	−0.65	+0.0031	+0.0059
μ	+1.91	+5.37	−0.57	−0.66	+0.0041	+0.0104
σ	2.44	4.29	0.46	0.64	0.0046	0.0091
t test	$p = 0.002$		$p = 0.616$		$p = 0.006$	
Levene's test	$F = 12.854$, $p = 0.001$		$F = 1.972$, $p = 0.168$		$F = 13.611$, $p = 0.001$	

TABLE 9. As in Table 8, but for tornadic and nontornadic events occurring ≥74.1 km (40 n mi) from the nearest radar.

	V_r (m s^{-1})		Diameter (km)		Shear (s^{-1})	
	Nontornadic	Tornadic	Nontornadic	Tornadic	Nontornadic	Tornadic
N	40	18	40	18	40	18
Median	+2.06	+1.93	−0.56	−0.56	+0.0019	+0.0015
μ	+2.63	+2.07	−0.48	−0.61	+0.0035	+0.0028
σ	2.98	3.17	0.53	0.53	0.0046	0.0042
t test	$p = 0.521$		$p = 0.392$		$p = 0.624$	
Levene's test	$F = 0.141$, $p = 0.708$		$F = 0.004$, $p = 0.949$		$F = 0.109$, $p = 0.743$	

to as a mesocyclonic VES to clarify its likely association with the mesocyclone.

The evaluation of all tornadic and nontornadic events required accurate storm motion vectors that were subtracted from the WSR-88D base velocity field. This allowed for proper measurement of the storm-relative midlevel inflow for mesocyclonic VES detection (e.g., Fig. 9). Analysis of the 34 tornadic events found that 20 events (58.8%) were identified as having a mesocyclonic VES in the 2.1–4.2-km layer preceding tornadogenesis. Maximum enhanced radial SRM values were observed between VS = −4 and −1. Of the 12 tornadic storms that lacked the identification of a mesocyclonic VES, 10 of the events were at least 120.4 km (65 n mi) from the nearest radar; moreover, all six tornadic events at a range of ≥129.6 km (70 n mi) failed to meet the criteria of having a mesocyclonic VES. Data quality and sampling issues prevented the analysis of the other two events. An example evolution of a tornadic supercell from Tropical Storm Andrea with a pronounced mesocyclonic VES is shown in Fig. 10. Enhanced SRM values of greater than 15.4 m s^{-1} (30 kt) were present as early as VS = −4, with the radial SRM values peaking at 28.5 m s^{-1} (55.3 kt) at VS = −2. The low-level mesocyclone strengthened and contracted prior to tornadogenesis following the peak intensity of the mesocyclonic VES. Analysis of the 90 nontornadic circulations found that 39 of the events (43.3%) were identified as having a mesocyclonic VES. This small percentage difference of having a mesocyclonic VES being detected in tornadic and nontornadic storms would mean that a mesocyclonic VES is not a stand-alone indicator for potential tornadogenesis.

c. *Reflectivity features*

Distinct inflow notches and appendage features, including hook echoes, were subjectively identified with 25 of the 34 tornadic events (73.5%); moreover, all tornadic storms lacking such supercellular features were at a range of ≥118.5 km (64 n mi) from the nearest radar. Data at the 0.5°-elevation angle are sampled at an elevation of approximately 1.85 km AGL at a range of

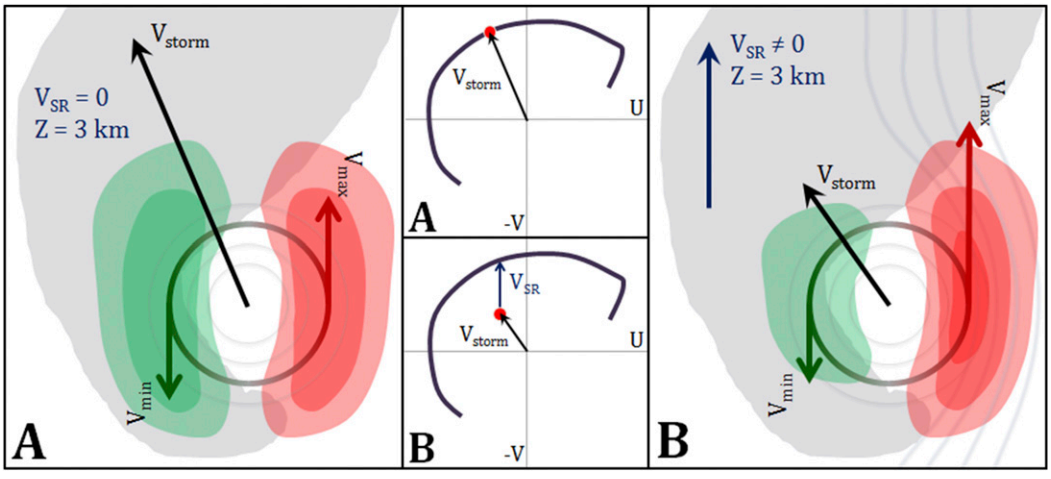

FIG. 8. Diagram of the storm-relative velocity field at a height of 3 km with an associated hodograph depicting V_{storm} for a supercell within (a) a V_{SR} that is zero and (b) a nonzero V_{SR}. The supercell diagrammed here was depicted as being north of a radar with V_{storm} denoted by a black arrow. Note that with the nonzero V_{SR} shown in B (blue arrow), the outbound velocity field (i.e., the flow into the supercell) appears greatly enhanced while the inbound velocity field appears reduced.

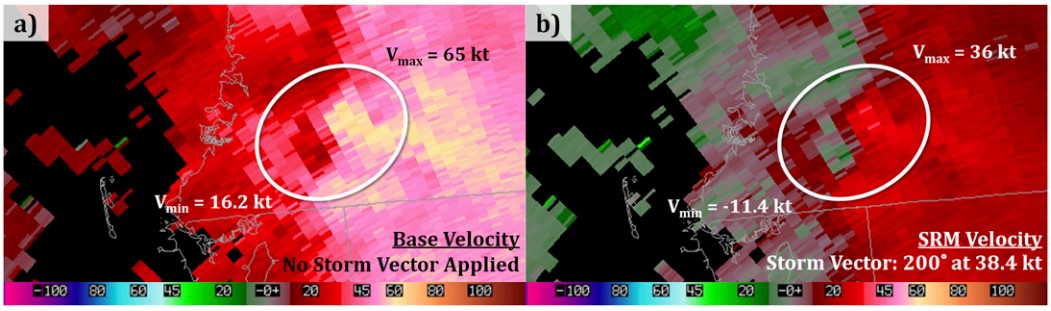

FIG. 9. (a) Base velocity and (b) SRM velocity depicting a mesocyclonic VES with the New Port Richey, FL, tornadic event during Tropical Storm Debby (event 16 in Table 1) from the 2.4°-elevation angle at 2111 UTC 24 Jun 2012. The Tampa Bay WSR-88D is located to the south-southeast of the storm. The base velocity field in (a) with no storm motion vector subtracted from it depicts the mesocyclone with outbound velocity values only. The SRM velocity field in (b) with the storm motion vector of 200° at 19.8 m s^{-1} (38.4 kt) subtracted from the base velocity field accurately depicts the asymmetric mesocyclone with representative inbound and outbound velocity values. The mesocyclonic VES is characterized by a V_{max} value of 18.5 m s^{-1} (36 kt) at a height of approximately 2.9 km (9.6 kft) AGL.

118.5 km; thus, the likelihood of observing supercellular features decreases with increasing distance from a radar, especially with storms that are shallow in depth, and suffering from increasing sample volume. The detection of supercell reflectivity features was also found to be increasingly difficult for convection in linear segments. Representative reflectivity profiles of tornadic convection at various ranges from the nearest radar are shown in Fig. 11. Inflow notches or appendage features were identified in 61 of the 90 nontornadic events analyzed (67.8%); however, 25% of nontornadic events within 118.5 km of the nearest radar did not exhibit any supercell reflectivity characteristics.

d. Dual-polarization analysis

Values and trends of the Z_{DR} and K_{DP} fields observed at the 0.5°-elevation angle found no distinction between tornadic and nontornadic events. Maximum Z_{DR} values ranged from <2.0 dB to >4.0 dB at VS = 0 regardless of tornadic potential. There were no discernible temporal trends for both tornadic and nontornadic events; however, the average maximum Z_{DR} values for tornadic storms remained 0.1–0.3 dB greater than for nontornadic storms. It should be noted that Z_{DR} values can change as much as ±1.5 dB from VS = −3 to 0. Maximum K_{DP} values and trends also showed no distinction between tornadic and nontornadic events. Maximum K_{DP} values were observed from <1.0° to 4.0° km^{-1}. The large range of K_{DP} and Z_{DR} values suggests that no minimum threshold value could be established for either product.

The work by Crowe et al. (2010) showed potential for utilizing the horizontal separation of greater Z_{DR} and K_{DP} values to determine the increased potential of tornadogenesis within TC convection. The three convective events analyzed by Crowe et al. (2010) showed that the separation of Z_{DR} and K_{DP} values was greater with the tornadic event; however, the sample size was very limited. More recent work by Gitro and Jurewicz (2016) demonstrated the utility of measuring Z_{DR} and K_{DP} separation in strong tornadic events with classic supercell storms and other non-TC events; however, there were challenges with the determination and quantification of this phenomenon with the shallow and more diminutive convection associated with TCs. The large range of maximum Z_{DR} and K_{DP} values observed in this study did not allow for a quantification of a threshold Z_{DR} or K_{DP} value to use, nor a percent below the maximum value to determine the areal coverage of the Z_{DR} and K_{DP} fields needed to assess any potential horizontal separation. Variations in storm size and structure also prevented any quantification of the distance or percent separation of the values at VS = 0 or over its temporal evolution.

The evaluation of the subjective identification of the horizontal separation of the Z_{DR} and K_{DP} extrema at the 0.5°-elevation angle provided little measure as a stand-alone indicator of identifying convection with increased tornadic potential. A distinct separation of greater Z_{DR} and K_{DP} values was found with 24 of the 34 tornadic events (70.6%), while 50 of the 90 nontornadic events (55.5%) exhibited similar horizontal separation; however, the separation of the Z_{DR} and K_{DP} fields appeared to be more pronounced in tornadic convection prior to tornadogenesis. The subjective identification of the separation of Z_{DR} and K_{DP} values was observed with convection up to 129.6 km (70 n mi) and, in some instances, beyond 129.6 km with both tornadic and nontornadic storms. The evolution of the horizontal separation of the Z_{DR} and K_{DP} values for a tornadic

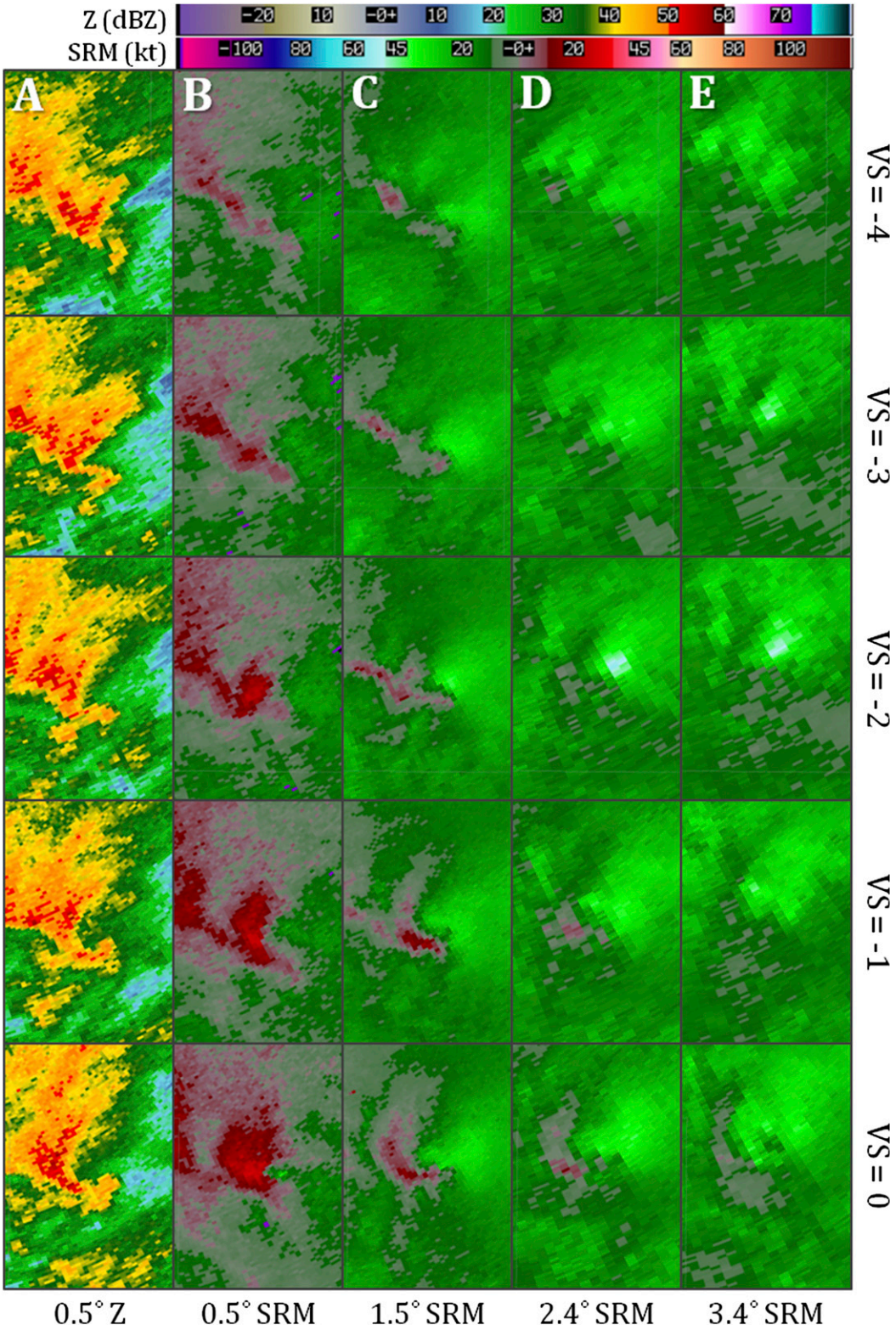

FIG. 10. Reflectivity Z at the 0.5°-elevation angle (column A) and SRM from select low-level elevation angles from 0.5° to 3.4° (columns B–E) from VS = −4 to 0 displaying the evolution of a mesocyclonic VES and low-level mesocyclone of the Myakka City, FL, tornado during Tropical Storm Andrea (event 1 in Table 2). The Tampa Bay WSR-88D is located to the north-northwest of the storm. The reflectivity (dB*Z*) and velocity (kt) color scales are located at the top of the image.

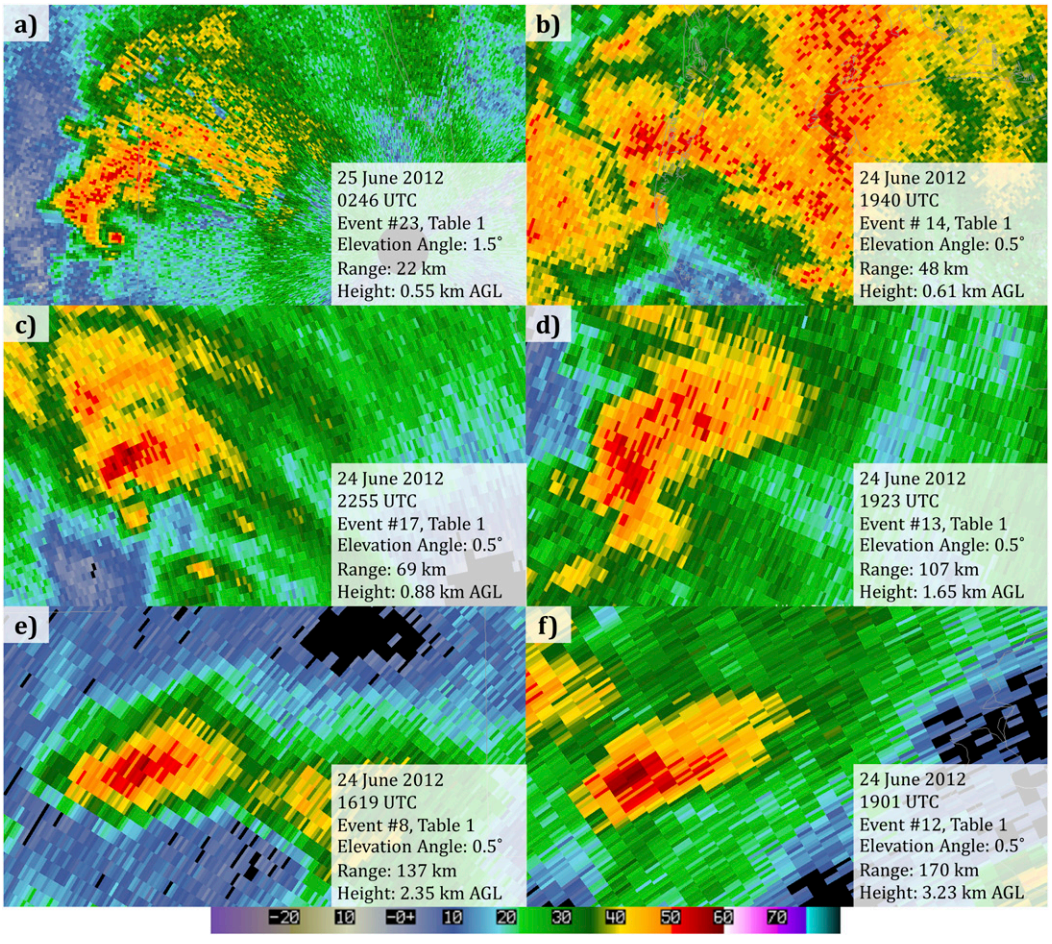

FIG. 11. Low-level reflectivity profiles of tornadic events from Tropical Storm Debby prior to tornadogenesis. (a)–(f) The convection shown increases in range from the radar. Information for each tornadic storm includes the date and time of the low-level scan, the corresponding event number from Table 1, the elevation angle of the reflectivity data, the range from the radar, and the height of the reflectivity data above ground level based on the location of the rotation feature.

event and a nontornadic event from VS = −2 to 0 is depicted in Fig. 12. Both storms were at a similar range from the radar, and similar Z_{DR} and K_{DP} values were sampled. The tornadic storm displayed a nearly complete separation of the two fields based on the coverage of Z_{DR} values > 2.0 dB and K_{DP} values > 1.0° km^{-1}. The nontornadic event showed a partial separation of the highlighted Z_{DR} and K_{DP} values by VS = 0.

5. Radar interrogation guidance

The analyses of the storm-scale characteristics noted distinguishable traits between tornadic and nontornadic events at ranges of 74.1 km (40 n mi) and 129.6 km (70 n mi) from the nearest radar; therefore, the development of a radar interrogation guidance will be defined by the following ranges: <74.1 km (<40 n mi), 74.1–129.6 km (40–70 n mi), and >129.6 km (>70 n mi). The analysis of the low-level rotational velocity characteristics found that all tornadic events had $V_r > 10.3\,m\,s^{-1}$ and shear across the rotation $> 0.010\,s^{-1}$ for convection within 74.1 km of the nearest radar, which matched results shown in previous studies; moreover, two-sample t tests showed statistically significant differences between the peak value and the rate of change for V_r and shear in this range. In contrast, tornadic events had a $V_r \geq 7.7\,m\,s^{-1}$ (15 kt) at the ranges of 74.1–129.6 and >129.6 km, and the shear across the rotation for most tornadic storms at these farther ranges was $<0.010\,s^{-1}$. There were also no significantly statistical differences between tornadic and nontornadic events at those ranges. The diameter of both tornadic and nontornadic circulations did contract in time; however, the analysis also showed there were no significant statistical differences with the diameter size or

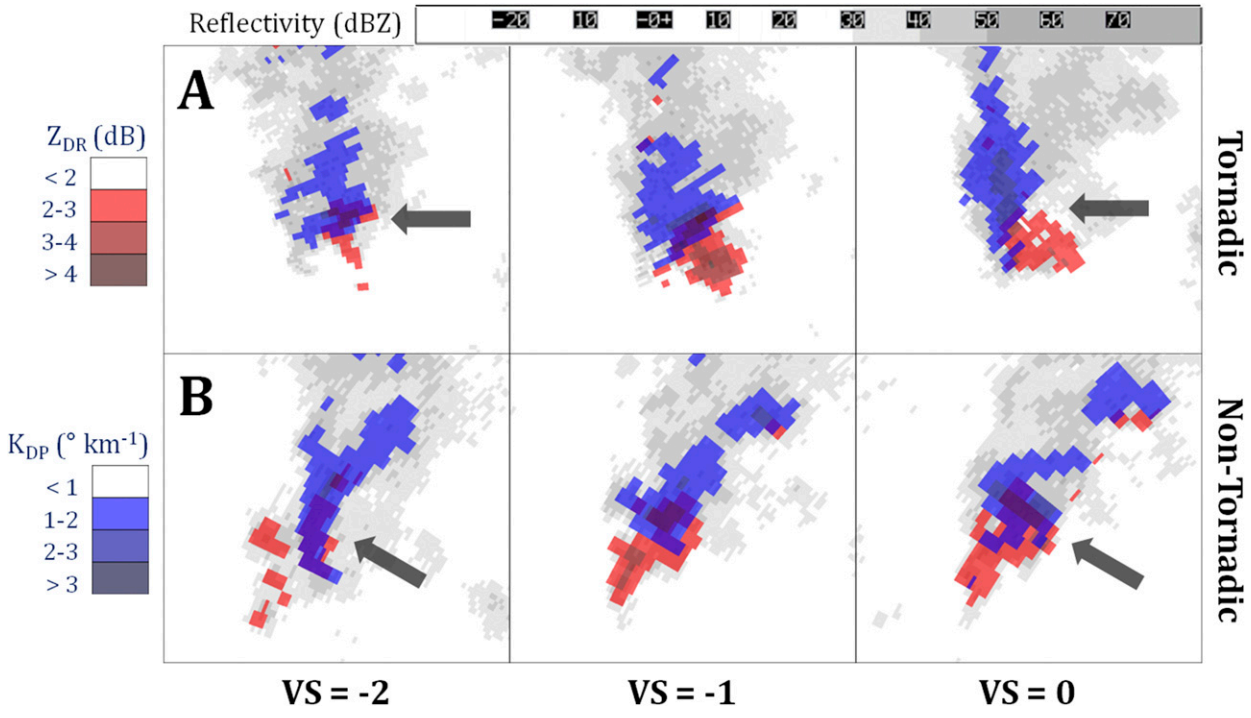

FIG. 12. Depiction of the horizontal separation of a Z_{DR} field of at least 2 dB (red) and a K_{DP} field of at least 1.0° km^{-1} (blue) of the Suwannee Springs, FL, tornadic event during Tropical Storm Andrea (row A, event 10 in Table 2) and a tornado-warned nontornadic storm observed by the Melbourne WSR-88D during Tropical Storm Andrea (row B) at the 0.5°-elevation angle. The evolution of the horizontal separation of the Z_{DR} and K_{DP} values for both storms are displayed from left to right from VS = −2 to 0 and are denoted by gray arrows at VS = −2 and 0. The reflectivity field of at least 30 dBZ is shown in grayscale in the background. The Z_{DR} and K_{DP} color scales are shown on the left, and the reflectivity grayscale is shown on top.

rate of size contraction of the low-level rotation at any range.

The evaluation of supercell reflectivity characteristics at the three different ranges from radar showed that all tornadic events had an identifiable supercell reflectivity signature at a range of <74.1 km, while 83% of nontornadic events also had identifiable supercell features (Fig. 13). The percent of storms with supercell echo

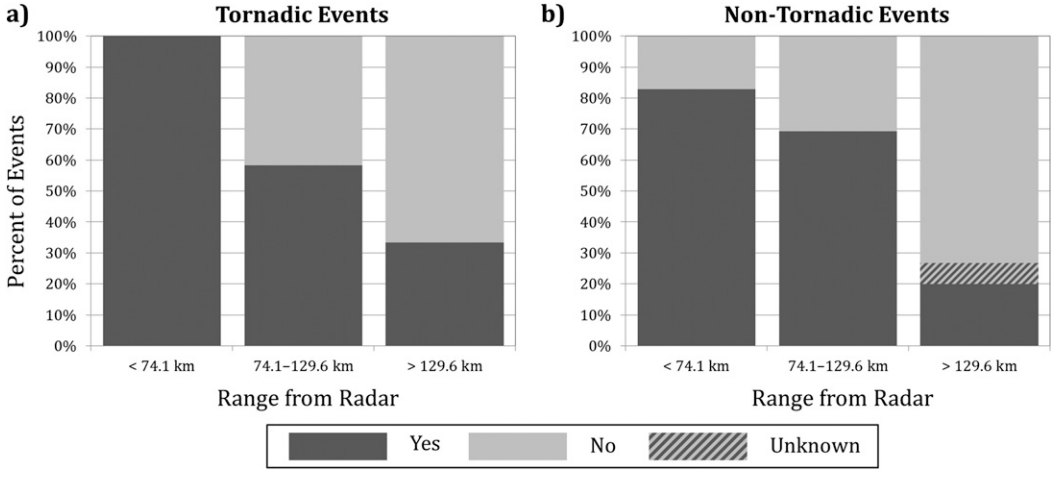

FIG. 13. Percent of (a) tornadic and (b) nontornadic events that exhibited supercell reflectivity signatures at the following ranges from the radar: <74.1, 74.1–129.6, and >129.6 km. Events marked as unknown were due to incomplete radar analysis from data quality or sampling challenges.

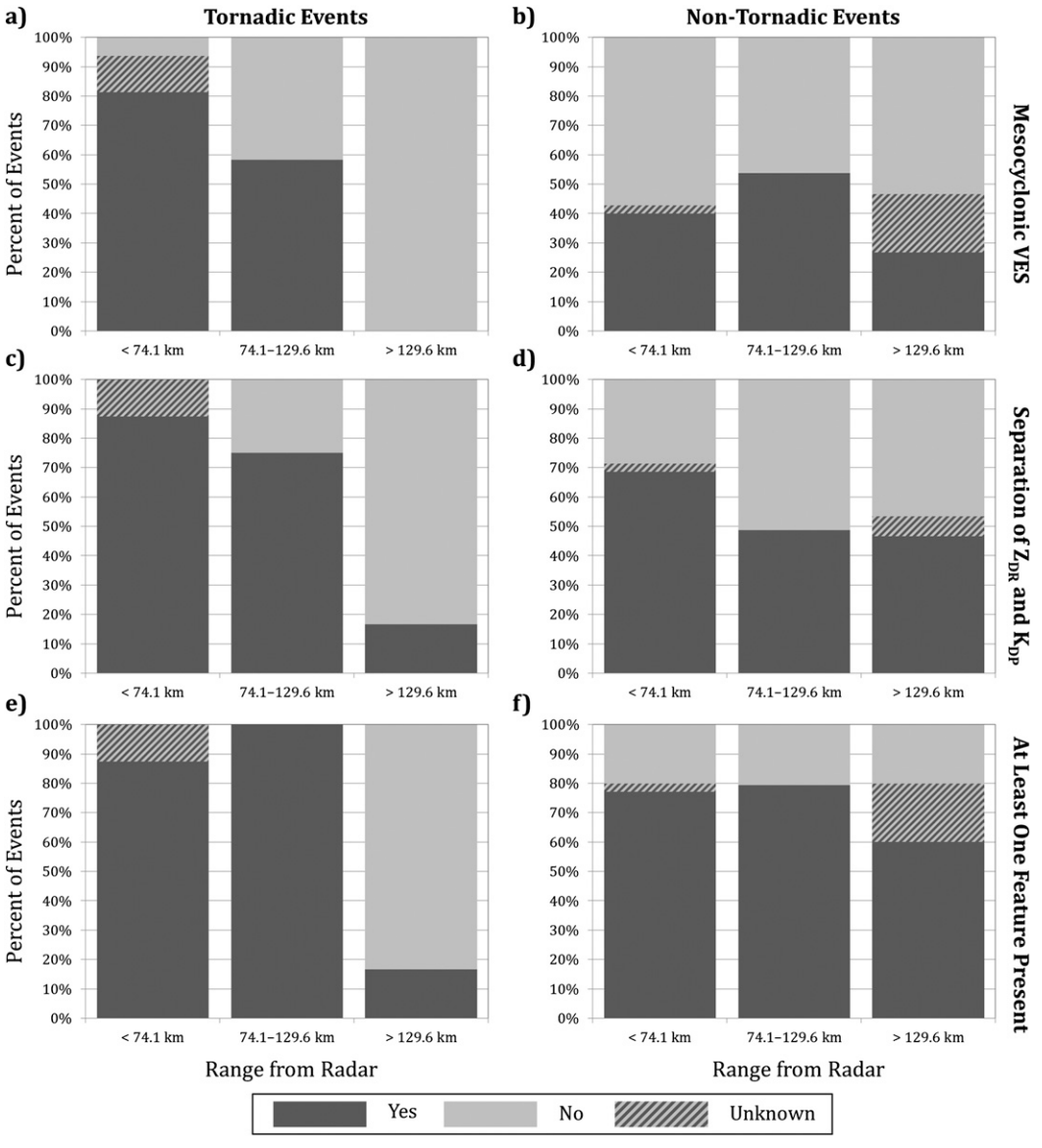

FIG. 14. Percent of (left) tornadic and (right) nontornadic events that were identified with (a),(b) a mesocyclonic VES, (c),(d) a horizontal separation of greater Z_{DR} and K_{DP} values, and (e),(f) at least one of the two features present at the following ranges from radar: <74.1, 74.1–129.6, and >129.6 km. Events marked as unknown were due to incomplete radar analysis from data quality or sampling challenges.

features decreased with range for both tornadic and nontornadic events, likely as a result of decreased sampling resolution and the radar overshooting these features with increasing range. Analysis of the detection of either a mesocyclonic VES or the horizontal separation of greater Z_{DR} and K_{DP} values at varying ranges from radar is shown in Fig. 14. All but one tornadic event that was fully analyzed had a mesocyclonic VES (Fig. 14a), and all tornadic events that were fully analyzed showed some horizontal separation of Z_{DR} and K_{DP} extrema (Fig. 14c). The detection of a mesocyclonic VES and horizontal separation of Z_{DR} and K_{DP} extrema also decreased with increasing range from radar. Since the stand-alone detection of a mesocyclonic VES or horizontal separation of Z_{DR} and K_{DP} extrema did not capture all tornadic events, the results were combined to see if having at least one of those two features present would provide increased confidence in determining the potential for tornadic development. The results showed that all tornadic storms up to a range of 129.6 km met the criteria (Fig. 14e), while only 74% of nontornadic storms up to a range of 129.6 km met the criteria (Fig. 14f).

TABLE 10. As in Table 1, but for the independent dataset containing the following TC events: Hurricane Arthur (2014), Tropical Storm Ana (2015), Tropical Storm Bill (2015), and Tropical Storm Colin (2016). The location column also lists the state for the nearest city to each tornado. Data related to these tornadic events were provided by NWS *Storm Data* through the NWS Performance Management System (https://verificaiton.nws.noaa.gov/). The time for event 3 was changed from 0325 to 0355 UTC to match the radar analysis.

Event No.	Time and date	Location	Duration (min)	Length (km)	Width (m)	Rating	Range (km)
			Hurricane Arthur (2014)				
1	2036 UTC 3 Jul	Rose Hill, NC	2	1.4	183	EF1	102
2	0050 UTC 4 Jul	Hamilton, NC	3	1.8	91	EF1	137
3	0355 UTC 4 Jul	California, NC	1	1.5	27	EF0	70
4	0515 UTC 4 Jul	Ocean Park, VA	1	0.5	27	EF0	80
5	0540 UTC 4 Jul	Norfolk, VA	1	0.4	27	EF0	67
			Tropical Storm Ana (2015)				
6	2110 UTC 11 May	Manteo, NC	1	0.8	27	EF0	165
			Tropical Storm Bill (2015)				
7	1925 UTC 17 Jun	Redland, OK	1	0.2	60	EF0	181
8	2220 UTC 17 Jun	Ben Bolt, TX	1	0.3	18	EF0	57
9	1009 UTC 18 Jun	Mansfield, LA	1	0.9	115	EF1	48
10	1138 UTC 18 Jun	Kickapoo, LA	5	5.6	174	EF1	30
			Tropical Storm Colin (2016)				
11	1925 UTC 6 Jun	Normandy, FL	10	6.3	165	EF1	26

These results suggested the following radar interrogation guidance for issuing a TOR for convection associated with TCs. For convection at a range $<$ 74.1 km from the nearest radar, the low-level rotation required a $V_r \geq 10.3\,\mathrm{m\,s^{-1}}$ (20 kt), shear across the rotation $\geq 0.010\,\mathrm{s^{-1}}$, and a contracting rotation diameter. The convection must exhibit supercell characteristics in the low-level reflectivity, and the convection must have acquired at least a mesocyclonic VES or an identifiable horizontal separation of greater Z_{DR} and K_{DP} values. For convection located at a range of 74.1–129.6 km from the nearest radar, convection is required to have a $V_r \geq 7.7\,\mathrm{m\,s^{-1}}$ (15 kt) and a contracting rotation diameter at the 0.5°-elevation angle. The convection does not require supercell reflectivity structure; however, a mesocyclonic VES or horizontal separation of greater Z_{DR} and K_{DP} values has to be present. For convection $>$ 129.6 km from the nearest radar, only a $V_r \geq 7.7\,\mathrm{m\,s^{-1}}$ (15 kt) at the 0.5°-elevation angle is required. No other velocity characteristics or storm-related features were shown to assist in identifying tornadic convection.

The performance of this radar interrogation guidance was evaluated using the events from Tropical Storms Debby and Andrea as well as an independent dataset. The independent dataset included 11 tornadic events and 38 nontornadic events from the following TCs: Hurricane Arthur (2014), Tropical Storm Ana (2015), Tropical Storm Bill (2015), and Tropical Storm Colin (2016). A list of all tornadoes verified by ground surveys is provided in Table 10. The calculated warning metrics for all tornado-warned events prior to applying the radar interrogation guidance, assuming one warning for each event, resulted in a POD of 0.889 and an FAR of 0.740 (Table 11). There were also five unwarned events within the independent dataset, of which the life cycle of two tornadoes occurred just prior to warning issuance.

Applying the radar interrogation guidance to the tornado-warned events from the six TC events reduced the number of false alarm events by 28.9% while improving the POD. Reexamination of all tornadic and nontornadic convection offered a clear analysis of 42 of the 45 tornadic storms. All 42 tornadic events that were fully examined resulted in the issuance of TORs. Three tornadic storms were plagued by data quality and radar-sampling challenges. Events impacted by poor data quality or sampling issues would have resulted in a TOR based on the assumption that other criteria not impacted by data quality and sampling issues were met. The combined POD was a perfect 1.000 (Table 12). The number of null events was reduced from 128 to 91 events, and this removal of 37 false alarm events reduced the combined FAR from 0.740 to 0.669 (Table 12).

TABLE 11. Number of verified, missed, and false alarm (null) events with Tropical Storm Debby (2012), Tropical Storm Andrea (2013), the independent dataset, and a combination of all datasets prior to the application of the proposed radar interrogation guidance. Also listed are the POD and FAR metrics, assuming that each warning decision contained one event.

	Verified	Missed	Null	POD	FAR
Debby (2012)	24	0	52	1.000	0.684
Andrea (2013)	10	0	38	1.000	0.792
Independent dataset	11	5	38	0.545	0.776
Combined	45	5	128	0.889	0.740

TABLE 12. Number of verified, missed, and false alarm (null) events with Tropical Storms Debby (2012) and Andrea (2013), the independent dataset, and a combination of all datasets after the application of the proposed radar interrogation guidance. Also listed are the POD and the FAR, along with the changes for each metric from before the application of the radar interrogation guidance (Table 11), assuming that each warning decision contained one event.

	Verified	Missed	Null	POD	POD difference	FAR	FAR difference
Debby (2012)	24	0	41	1.000	0.000	0.631	−0.053
Andrea (2013)	10	0	22	1.000	0.000	0.688	−0.104
Independent dataset	11	0	28	1.000	+0.455	0.718	−0.058
Combined	45	0	91	1.000	+0.111	0.669	−0.071

Numerous challenges and other radar settings can impact the interrogation of TC convection for tornadic potential. Limitations with radar detection and potential data quality issues, such as range folding and ground clutter, were found to hinder proper analysis of some events. The identification and assessment of a mesocyclonic VES are dependent upon the viewing angle from the radar with respect to the storm inflow region and the application of a proper storm motion for SRM analysis. The determination of horizontal separation of greater Z_{DR} and K_{DP} extrema are subjective given the varying ranges of both Z_{DR} and K_{DP} extrema from storm to storm and even during the evolution of each storm. Given these radar challenges, the recommendations are provided as guidance only and not as strict thresholds. For best judgment, one should consider all radar-based parameters as well as the mesoscale environment in the warning decision-making process.

6. Summary

Operational interrogation and warning decision-making for tornadic development present a great challenge for forecasters during a multihazard TC event. When compared with classic Great Plains supercells, TC convective storms are shallower in depth and the supercellular features are subtle, if present at all. Rotational signatures are also generally weaker. Tornadogenesis can occur quite rapidly, and TC tornadoes often exist for only a few minutes. This study utilized two significant tornado outbreaks attributed to TC events to compile radar-based interrogation guidance using superresolution and dual-polarization data from the WSR-88D radar network.

A total of 34 tornadic events and 90 nontornadic events from Tropical Storms Debby (2012) and Andrea (2013) were evaluated to determine if there are velocity and other storm-scale properties that can assist in delineating tornadic events prior to tornadogenesis. Statistically significant differences were found with the low-level V_r and shear across the rotation at a range of <74.1 km (40 n mi). Other differences were noted regarding the percentage of storms exhibiting supercell reflectivity signatures, midlevel mesocyclone VES, and horizontal separation of Z_{DR} and K_{DP} extrema. Greater challenges existed in distinguishing potentially tornadic storms from nontornadic storms at longer ranges from the nearest radar as a result of radar-sampling challenges. Radar-based interrogation guidance was established from the resulting analyses. The guidance offered by the author improved the POD for the independent dataset; moreover, the number of false alarm events for the tornadic storms of Tropical Storms Debby and Andrea and the independent dataset was reduced by 28.9%. The FAR was reduced to 0.669, which is below the 2013 NWS GPRA FAR performance metric goal of 0.72.

Findings from this study along with the associated radar interrogation guidance were used to develop training for NWS operational forecasters. A series of online training modules focusing on TC tornadoes were delivered by the Warning Decision Training Division (WDTD), including a lesson dedicated to real-time operational radar interrogation (available online at http://www.wdtd.noaa.gov). Forecasters also had the ability to apply the radar interrogation guidance to potentially tornadic storms from Tropical Storm Andrea in a WES application on the AWIPS platform.

Technological advancements for operational forecasters can also improve the interrogation process for identifying potentially tornadic storms. It was noted that potentially tornadic convection was shown to have a greater rate of increase in the low-level V_r and shear across the rotation; however, this might be challenging to evaluate in real time. New tools, such as the Tracking Meteogram tool for AWIPS, could allow forecasters to analyze the time series of radar-derived trends of storm-scale velocity characteristics (Burks and Sperow 2015). The inclusion of additional scans at the lowest elevation angle through the Supplemental Adaptive Intravolume Low-Level Scan (SAILS) and the Multiple Elevation Scan Option for SAILS (MESO-SAILS) options with the WSR-88D network can allow forecasters to better monitor low-level storm-scale features (ROC 2014). As radar products and scanning strategies evolve, future

evaluations of TC tornado events can assist in determining new methodologies for better delineating between tornadic and nontornadic events to improve the FAR without compromising POD.

Acknowledgments. The author thanks the anonymous reviewers for their comments, insight, and feedback. The author also thanks Dr. Pamela Heinselman from the NOAA/OAR/National Severe Storms Laboratory (NSSL) for her insight and review, Brad Grant (NWS/WDTD) and James LaDue (NWS/WDTD) for their review of this work and the associated training deliverables, and Eric Jacobsen (CIMMS/OU and NWS/WDTD) for providing the radar data for the independent evaluations. Funding was provided by NOAA/Office of Oceanic and Atmospheric Research under NOAA–University of Oklahoma Cooperative Agreement NA11OAR4320072, U.S. Department of Commerce.

REFERENCES

Beven, J. L., 2013: Tropical Storm Andrea. NOAA/National Hurricane Center Tropical Cyclone Rep., 33 pp. [Available online at http://www.nhc.noaa.gov/data/tcr/AL012013_Andrea.pdf.]

Brandes, E. A., 1977: Flow in severe thunderstorms observed by dual-Doppler radar. *Mon. Wea. Rev.*, **105**, 113–120, doi:10.1175/1520-0493(1977)105<0113:FISTOB>2.0.CO;2.

——, 1978: Mesocyclone evolution and tornadogenesis: Some observations. *Mon. Wea. Rev.*, **106**, 995–1011, doi:10.1175/1520-0493(1978)106<0995:MEATSO>2.0.CO;2.

——, 1984: Relationship between radar-derived thermodynamic variables and tornadogenesis. *Mon. Wea. Rev.*, **112**, 1033–1052, doi:10.1175/1520-0493(1984)112<1033:RBRDTV>2.0.CO;2.

Brown, R. A., V. T. Wood, R. M. Steadham, R. R. Lee, B. A. Flickinger, and D. Sirmans, 2005: New WSR-88D volume coverage pattern 12: Results of field tests. *Wea. Forecasting*, **20**, 385–393, doi:10.1175/WAF848.1.

Bunkers, M. J., B. A. Klimowski, J. W. Zeitler, R. L. Thompson, and M. L. Weisman, 2000: Predicting supercell motion using a new hodograph technique. *Wea. Forecasting*, **15**, 61–79, doi:10.1175/1520-0434(2000)015<0061:PSMUAN>2.0.CO;2.

Burgess, D. W., R. J. Donaldson, and P. R. Desrochers, 1993: Tornado detection and warning by radar. *The Tornado: Its Structure, Dynamics, Predictions and Hazards*, *Geophys. Monogr.*, Vol. 79, Amer. Geophys. Union, 203–211.

Burks, J. E., and K. Sperow, 2015: The Tracking Meteogram, an AWIPS II tool for time-series analysis. *31st Conf. on Environmental Information Processing Technologies*, Phoenix, AZ, Amer. Meteor. Soc., 15B.3. [Available online at https://ams.confex.com/ams/95Annual/webprogram/Paper266464.html.]

Crowe, C. C., W. A. Petersen, L. D. Carey, and D. J. Cecil, 2010: A dual-polarization investigation of tornado-warned cells associated with Hurricane Rita (2005). *Electron. J. Oper. Meteor.*, **11** (4). [Available online at http://nwafiles.nwas.org/ej/pdf/2010-EJ4.pdf.]

Crum, T. D., R. L. Alberty, and D. W. Burgess, 1993: Recording, archiving, and using WSR-88D data. *Bull. Amer. Meteor. Soc.*, **74**, 645–653, doi:10.1175/1520-0477(1993)074<0645:RAAUWD>2.0.CO;2.

Curtis, L., 2004: Midlevel dry intrusions as a factor in tornado outbreaks associated with landfalling tropical cyclones from the Atlantic and Gulf of Mexico. *Wea. Forecasting*, **19**, 411–427, doi:10.1175/1520-0434(2004)019<0411:MDIAAF>2.0.CO;2.

Dawson, D. T., E. R. Mansell, and M. R. Kumjian, 2015: Does wind shear cause hydrometeor size sorting? *J. Atmos. Sci.*, **72**, 340–348, doi:10.1175/JAS-D-14-0084.1.

Desrochers, P. R., and F. I. Harris, 1996: Interpretation of mesocyclone vorticity and divergence structure from single-Doppler radar. *J. Appl. Meteor.*, **35**, 2191–2209, doi:10.1175/1520-0450(1996)035<2191:IOMVAD>2.0.CO;2.

Devanas, A. D., D. Gregoria, K. B. Kasper, and P. Santos, 2008: Tropical cyclone induced tornadoes associated with the formation of Tropical Storm Barry. *Tropical Meteorology Special Symp./20th Conf. on Climate Variability and Change*, New Orleans, LA, Amer. Meteor. Soc., JP3.16. [Available online at https://ams.confex.com/ams/pdfpapers/131758.pdf.]

Edwards, R., A. R. Dean, R. L. Thompson, and B. T. Smith, 2012: Convective modes for significant severe thunderstorms in the contiguous United States. Part III: Tropical cyclone tornadoes. *Wea. Forecasting*, **27**, 1507–1519, doi:10.1175/WAF-D-11-00117.1.

Gitro, C. M., and M. L. Jurewicz, 2016: The utility of considering ZDR and KDP signatures in the tornado warning process. Part II: Discriminating between tornadic and non-tornadic storms in high-end severe weather events. Preprints, *41st NWA Annual Meeting*, Norfolk, VA, National Weather Association, 3A.6.

Kimberlain, T. B., 2013: Tropical Storm Debby. NOAA/National Hurricane Center Tropical Cyclone Rep., 51 pp. [Available online at http://www.nhc.noaa.gov/data/tcr/AL042012_Debby.pdf.]

Kumjian, M. R., and A. Ryzhkov, 2008: Polarimetric signatures in supercell thunderstorms. *J. Appl. Meteor.*, **47**, 1940–1961, doi:10.1175/2007JAMC1874.1.

——, and ——, 2009: Storm-relative helicity revealed from polarimetric radar measurements. *J. Atmos. Sci.*, **66**, 667–685, doi:10.1175/2008JAS2815.1.

Leifer, M. C., V. Chandrasekar, and E. Perl, 2013: Dual polarization implementation approaches and geometry trades for multifunctional phased array radar (MPAR). *36th Conf. on Radar Meteorology*, Breckenridge, CO, Amer. Meteor. Soc., 161. [Available online at https://ams.confex.com/ams/36Radar/webprogram/Paper229149.html.]

Levene, H., 1960: Robust tests for equality of variances. *Contributions to Probability and Statistics: Essays in Honor of Harold Hotelling*, I. Olkin et al., Eds., Stanford University Press, 278–292.

Magsig, M. A., and E. M. Page, 2002: Development and implementation of the NWS warning event simulator version 1.0. Preprints, *18th Int. Conf. on Interactive Information Processing Systems*, Orlando, FL, Amer. Meteor. Soc., J8.10. [Available online at https://ams.confex.com/ams/pdfpapers/27993.pdf.]

——, N. M. Said, N. L. Levit, and X. Yu, 2004: The Weather Event Simulator and opportunities for the severe storms community. *22nd Conf. Severe Local Storms*, Miami, FL, Amer. Meteor. Soc., P2.1. [Available online at https://ams.confex.com/ams/11aram22sls/webprogram/Paper82007.html.]

——, T. Decker, and N. M. Said, 2006: Builds five and six of NOAA's Weather Event Simulator. *18th Int. Conf. on Interactive Information Processing Systems*, Atlanta, GA, Amer. Meteor. Soc., P7.7. [Available online at https://ams.confex.com/ams/Annual2006/webprogram/Paper104624.html.]

McCaul, E. W., Jr., D. E. Buechler, S. J. Goodman, and M. Cammarata, 2004: Doppler radar and lightning network observations of a severe outbreak of tropical cyclone tornadoes. *Mon. Wea. Rev.*, **132**, 1747–1763, doi:10.1175/1520-0493(2004)132<1747:DRALNO>2.0.CO;2.

Nolan, D. S., 2004: Vortex sheets, vortex rings, and a mesocyclone. *22nd Conf. on Severe Local Storms*, Miami, FL, Amer. Meteor. Soc., 14.1. [Available online at https://ams.confex.com/ams/11aram22sls/techprogram/paper_81516.htm.]

NWS, 2012: Hurricane Irene, August 21–30, 2011. NOAA/NWS Service Assessment, 129 pp. [Available online at http://www.nws.noaa.gov/om/assessments/pdfs/Irene2012.pdf.]

Rappaport, E. N., 2014: Fatalities in the United States from Atlantic tropical cyclones: New data and interpretation. *Bull. Amer. Meteor. Soc.*, **95**, 341–346, doi:10.1175/BAMS-D-12-00074.1.

ROC, 2014: MESO-SAILS (Multiple Elevation Scan Option for SAILS) initial description document. NOAA/NWS/Radar Operations Center, 4 pp. [Available online at https://www.roc.noaa.gov/wsr88d/PublicDocs/NewTechnology/MESO-SAILS_Intial_Description_v02_Feb_2014.pdf.]

Romine, G. S., D. W. Burgess, and R. B. Wilhelmson, 2008: A dual-polarization-radar-based assessment of the 8 May 2003 Oklahoma City area tornadic supercell. *Mon. Wea. Rev.*, **136**, 2849–2870, doi:10.1175/2008MWR2330.1.

Rotunno, R., 1984: An investigation of a three-dimensional asymmetric vortex. *J. Atmos. Sci.*, **41**, 283–298, doi:10.1175/1520-0469(1984)041<0283:AIOATD>2.0.CO;2.

——, and J. B. Klemp, 1982: The influence of the shear-induced pressure gradient of thunderstorm motion. *Mon. Wea. Rev.*, **110**, 136–151, doi:10.1175/1520-0493(1982)110<0136:TIOTSI>2.0.CO;2.

——, and ——, 1985: On the rotation and propagation of simulated supercell thunderstorms. *J. Atmos. Sci.*, **42**, 271–292, doi:10.1175/1520-0469(1985)042<0271:OTRAPO>2.0.CO;2.

Schneider, D., and S. Sharp, 2007: Radar signatures of tropical cyclone tornadoes in central North Carolina. *Wea. Forecasting*, **22**, 278–286, doi:10.1175/WAF992.1.

Schultz, L. A., and D. J. Cecil, 2009: Tropical cyclone tornadoes, 1950–2007. *Mon. Wea. Rev.*, **137**, 3471–3484, doi:10.1175/2009MWR2896.1.

Spratt, S. M., D. W. Sharp, P. Welsh, A. Sandrik, F. Alsheimer, and C. Paxton, 1997: A WSR-88D assessment of tropical cyclone outer rainband tornadoes. *Wea. Forecasting*, **12**, 479–501, doi:10.1175/1520-0434(1997)012<0479:AWAOTC>2.0.CO;2.

Torres, S. M., and C. D. Curtis, 2007: Initial implementation of super-resolution data on the NEXRAD network. *23rd Conf. on International Interactive Information and Processing Systems (IIPS) for Meteorology, Oceanography, and Hydrology*, San Antonio, TX, Amer. Meteor. Soc., 5B.10. [Available online at http://ams.confex.com/ams/87ANNUAL/techprogram/paper_116240.htm.]

Vescio, M. D., S. J. Weiss, and F. P. Ostby, 1996: Tornadoes associated with Tropical Storm Beryl. *Natl. Wea. Assoc. Dig.*, **21** (1), 2–10.

Weisman, M. L., and J. B. Klemp, 1984: The structure and classification of numerically simulated convective storms in directionally varying wind shears. *Mon. Wea. Rev.*, **112**, 2479–2498, doi:10.1175/1520-0493(1984)112<2479:TSACON>2.0.CO;2.